A&A 601, A119 (2017)
DOI: 10.1051/0004-6361/201629854

Astronomy & Astrophysics

An abundance analysis from the STIS-HST UV spectrum of the non-magnetic Bp star HR 6000

F. Castelli[1], C. R. Cowley[2], T. R. Ayres[3], G. Catanzaro[4], and F. Leone[4,5]

[1] Istituto Nazionale di Astrofisica, Osservatorio Astronomico di Trieste, via Tiepolo 11, 34143 Trieste, Italy
e-mail: castelli@oats.inaf.it
[2] Department of Astronomy, University of Michigan, Ann Arbor, MI 48109-1042, USA
[3] Center for Astrophysics and Space Astronomy, University of Colorado, Boulder, CO 80309-0389, USA
[4] Istituto Nazionale di Astrofisica, Osservatorio Astronomico di Catania, via S. Sofia 78, 95123 Catania, Italy
[5] Universita' di Catania, Dipartimento di Fisica e Astronomia, Sezione Astrofisica, via S. Sofia 78, 95123 Catania, Italy

Received 6 October 2016 / Accepted 6 December 2016

ABSTRACT

Context. The sharp-line spectrum of the non-magnetic, main-sequence Bp star HR 6000 has peculiarities that distinguish it from those of the HgMn stars with which it is sometimes associated. The position of the star close to the center of the Lupus 3 molecular cloud, whose estimated age is on the order of 9.1 ± 2.1 Myr, has lead to the hypothesis that the anomalous peculiarities of HR 6000 can be explained by the young age of the star.
Aims. Observational material from the *Hubble* Space Telescope (HST) provides the opportunity to extend the abundance analysis previously performed for the optical region and clarify the properties of this remarkable peculiar star. Our aim was to obtain the atmospheric abundances for all the elements observed in a broad region from 1250 to 10 000 Å.
Methods. An LTE synthetic spectrum was compared with a high-resolution spectrum observed with the Space Telescope Imaging Spectrograph (STIS) equipment in the 1250−3040 Å interval. Abundances were changed until the synthetic spectrum fit the observed spectrum. The assumed model is an LTE, plane-parallel, line-blanketed ATLAS12 model already used for the abundance analysis of a high-resolution optical spectrum observed at ESO with the Ultraviolet and Visual Echelle Spectrograph (UVES). The stellar parameters are $T_{\rm eff}$ = 13450 K, $\log g$ = 4.3, and zero microturbulent velocity.
Results. Abundances for 28 elements and 7 upper limits were derived from the ultraviolet spectrum. Adding results from previous work, we have now quantitative results for 37 elements, some of which show striking contrasts with those of a broad sample of HgMn stars. The analysis has pointed out numerous abundance anomalies, such as ionization anomalies and line-to-line variation in the derived abundances, in particular for silicon. The inferred discrepancies could be explained by non-LTE effects and with the occurrence of diffusion and vertical abundance stratification. In the framework of the last hypothesis, we obtained, by means of trial and error, empirical step functions of abundance versus optical depth $\log(\tau_{5000})$ for carbon, nitrogen, silicon, manganese, and gold, while we failed to find such a function for phosphorous. The poor results for carbon, and mostly for phosphorus, suggest the possible importance in this star of NLTE effects to be investigated in future works.

Key words. stars: abundances – stars: atmospheres – stars: chemically peculiar – stars: individual: HR 6000

1. Introduction

The ASTRAL spectral library for hot stars (Ayres et al. 2014) includes observations of the peculiar star HR 6000 (HD 144667), giving us the possibility of studying at high resolution the ultraviolet spectrum of this special peculiar star for the first time after the International Ultraviolet Explorer (IUE) era. The star is anomalous because it does not fit into any of the typical CP subclasses, but seems to combine abundance anomalies from several Bp subtypes (Andersen et al. 1984). A remarkable characteristic is the extreme deficiency of silicon, which makes HR 6000 the most deficient silicon star of the HgMn group, with which it is usually associated.

Peculiarities in the spectrum of HR 6000 were first noted by Bessell & Eggen (1972), who classified it as a peculiar main-sequence B star with strong P II lines and weak helium (see also van den Ancker et al. 1996). This star is the brighter, more massive component of the visual binary system Δ199 or Dunlop 199 (Dunlop 1829). The second component is the Herbig Ae star HR 5999 (HD 144668) (Eggen 1975). Because the Δ199 double system is located close to the center of the Lupus 3 molecular cloud, which is populated by numerous TTauri stars, it has been assumed that the system is the same age as the cloud, i.e., about (9.1 ± 2.1) Myr (James et al. 2006). In this case, HR 6000 is a very young peculiar star and its anomalous peculiarity could be explained by its young age. The spectrum of HR 6000 also seems to be polluted by lines of some cool star. The identification of an unshifted Li I line at 6707.7 Å led Castelli & Hubrig (2007) to support the hypothesis from van den Ancker et al. (1996) of the presence of a faint TTauri companion, which could be either physically related to HR 6000 to form a close binary system or located in the foreground of HR 6000.

After recognition of its peculiar nature, the first high-resolution studies of the chemical composition of HR 6000 were of an ultraviolet spectrum obtained with IUE in the far and near ultraviolet on March 1979 (Castelli et al. 1981, 1985) and an optical spectrum observed at ESO with a dispersion of 12 Å mm^{-1} covering the spectral range $\lambda\lambda$ 3323−5316 Å (Andersen & Jaschek 1984).

While very significant qualitative results on the nature of the star were provided from the optical spectra by Andersen et al. (1984), the quantitative analysis from the IUE spectra (Castelli et al. 1985) has given abundances for almost all the elements observed in the IUE range (1258−1960 Å and 2050−3150 Å), but with large uncertainties. The quantitative analysis of the IUE spectra was a very difficult task, in particular owing to the rather low resolving power and poor signal-to-noise ratio (S/N), severe line crowding, and poor quality of the line lists available at that time for computing synthetic spectra. However, the underabundance of several elements (Be, C, N, Mg, Al, Si, S, Sc, Co, Ni, Cu, and Zn) and overabundance of others elements (B, P, Ca, Mn, Fe, and Ga) were determined. For a few elements, spurious high abundances were assigned owing to several unresolved blended features and unidentified components.

Later on, in a series of papers, Smith (1993, 1994, 1997) and Smith & Dworetsky (1993) published the abundances of selected elements obtained from IUE spectra of a sample of HgMn stars, including HR 6000, which they noted did not fit the typical abundance pattern. They pointed out three additional stars, 33 Gem, 36 Lyn, and 46 Aql, with abundances that depart from the more general behavior observed in the majority of the HgMn class members.

A comparison of the Smith and Smith & Dworetsky results with those from Castelli et al. (1985) for the elements in common (Mg II, Cr II, Mn II, Fe II, Ni II, Zn II) has shown agreement within the error limits for all the elements except for Zn II whose abundance was estimated −8.3 dex by Castelli et al. (1985) and −9.2 dex by Smith (1994). We currently adopt an upper limit of −8.84 for Zn.

Several years later, high-resolution optical spectra became available to study HR 6000 in the visual range. Catanzaro et al. (2004) analyzed the 3800−7000 Å region on FEROS spectra observed with 48 000 resolving power, while Castelli & Hubrig (2007) and Castelli et al. (2009) studied the 3040−10 000 Å region on a spectrum observed at ESO with the Ultraviolet and Visual Echelle Spectrograph (UVES) at a resolving power ranging from 80 000 to 110 000. The comparison of the abundances derived from the FEROS and UVES spectra were in rather good agreement, with discrepancies larger than 0.3 dex only for He I, Mg II, and Mn II. For iron the difference was 0.3 dex. In both analyses there are only upper limits for a few elements. Discordant abundances from the visual and ultraviolet spectra were found for O I, S II, and Ti II. In Castelli & Hubrig (2007) several studies on the nature of the star are quoted, included those on variability. While a weak photometric variability was pointed out by van den Ancker et al. (1996) and by Kurtz & Marang (1995), no spectroscopic variability was evident from the different spectra taken by Andersen & Jaschek (1984) and Castelli & Hubrig (2007) at different epochs and with different instruments.

The Space Telescope Imaging Spectrograph (STIS) ultraviolet spectrum of the ASTRAL library gives us the opportunity to extend the UVES observations to the ultraviolet and supersede the low quality IUE data. The entire range from 1250 to 10 000 Å is now covered by high-resolution spectra of HR 6000. The presence of elements not observed in the optical region and elements that are present in the ultraviolet with more ionization states and more lines allow us to improve the investigation of effects related to the atomic diffusion (Michaud 1970), in particular, vertical abundance stratification.

The first theoretical attempt to point out the effect of abundance stratification on line profiles is from Alecian & Artru (1988) who analyzed the case of the Ga II resonance line at 1414.401 Å in the atmospheres of Ap stars. Babel (1994) explained the Ca II profile at 3933 Å observed in Ap stars with the help of a step function of the calcium abundance versus optical depth. Leone & Lanzafame (1997) and Leone (1998) introduced the use of the contribution functions to associate abundances with atmospheric layers. In addition, Leone et al. (1997) and Catanzaro et al. (2016) extended the search for vertical abundance stratification to the ultraviolet.

All the previous studies tell us that in peculiar stars with low rotational velocity and no convective motions, such as in HR 6000, vertical abundance stratification for certain elements may be present near the surface. Currently several studies have been performed with the aim of detecting vertical stratification of the abundances. In this context, of particular interest is the VeSE1kA project (LeBlanc et al. 2015). This paper could add some more information related to the abundance peculiarities observed in HgMn stars.

2. Observations

HR 6000 is one of the targets included in the Hot Stars part of the HST Cycle 21 "Advanced Spectral Library (ASTRAL)" Project (Ayres et al. 2014: GO-13346). The star was observed several days in October 2014 with moderate and high-resolution echelle settings of STIS. The final spectrum covers the range 1150−3045 Å. The nominal resolving power R ranges from about 30 000 to 110 000; the S/N typically is greater than 100, approaching 200 in selected regions. We used the final spectrum that resulted from the calibration and merging of the overlapping echelle spectra observed in the different wavelength intervals, as performed by the ASTRAL Science Team[1].

For this work we analyzed the whole region from 1250 to 3045 Å, using the IRAF tool "continuum" to normalize the observed spectrum to the continuum level. When we compared observed and computed spectra, we tentatively fixed different resolving powers for the different intervals corresponding roughly to major switches in the echelle modes. While the theoretical resolving powers of the moderate-resolution far-ultraviolet E140M and moderate-resolution near-UV E230M echelle modes are 45 000 and 30 000, respectively (Ayres 2010), measurements of narrow features in the HR 6000 spectrum suggest lower effective resolutions of 30 000 and 25 000, respectively. However, at the longer wavelengths (>2300 Å) recorded with the NUV high-resolution echelle E230H, there appears to be little degradation of the theoretical resolving power of 110 000. The cause of the resolution decrease for the medium-resolution spectra is unknown, but currently is under investigation. The wavelength scale of the STIS spectra are provided in vacuum for the whole observed region. We converted the wavelength scale of the final spectrum from vacuum to air for the 2000−3040 Å interval.

3. The analysis

Abundances were determined with the synthetic spectrum method by changing the abundance of a given element until agreement between observed and computed profiles is obtained. We used the SYNTHE code (Kurucz 2005) to compute local thermodynamic equilibrium (LTE) synthetic spectra when the adopted abundance is constant with depth and a modified version of SYNTHE (Kurucz, priv. comm.) when a vertical abundance stratification is considered for a given element.

[1] http://casa.colorado.edu/~ayres/ASTRAL/

To be consistent with a previous abundance analysis performed on an UVES optical spectrum by Castelli et al. (2009), we adopted the same model atmosphere without any modification. It is a plane-parallel, LTE model atmosphere with parameters $T_{\rm eff}$ = 13 450 K, log g = 4.3, and microturbulent velocity ξ = 0.0 km s^{-1}, computed with the ATLAS12 code (Kurucz 2005) for the individual abundances of HR 6000, as derived from the optical spectrum and tabulated in Castelli et al. (2009). In all the computations the continuous opacity includes the scattering contribution from electron scattering and Rayleigh scattering from neutral hydrogen, neutral helium, and molecular hydrogen H_2. Hydrogen Rayleigh scattering, which is an important opacity source for modeling Lyman$_\alpha$ wings, was computed according to Gavrila (1967). The other scattering sources are described in Kurucz (1970). No scattering was considered in the line source function, which was approximated with the Planck function.

The model parameters are updated values from those derived by Castelli & Hubrig (2007) from both Balmer profiles and the Fe I and Fe II ionization equilibrium. In Castelli et al. (2009) $T_{\rm eff}$ and log g were obtained from Strömgren photometry, from the requirement that there is no correlation between the Fe II abundances derived from high- and low-excitation lines, and from the constraint of Fe I–Fe II ionization equilibrium. The only element used to fix the model parameters was iron because other elements were not observed in different ionization degrees in the optical spectrum, except for phosphorous, which was present with P II and P III lines. Owing to the larger number of lines and more trustworthy atomic data for both Fe I and Fe II lines than for phosphorous, in particular P III, we preferred to use iron to phosphorous for the determination of the model parameters.

As discussed in Castelli et al. (2009), the Balmer lines were no longer used owing to the several problems related with the UVES spectra in the regions of the Balmer lines.

The computed spectrum was broadened for a rotational velocity $v \sin i$ = 1.5 km s^{-1} and a Gaussian instrumental profile corresponding to different resolving powers for different intervals, as indicated in Sect. 2. In order to superimpose the observed profiles on the computed profiles the observed spectrum was shifted by a velocity ranging from 0.0 km s^{-1} at 1250 Å to 2.0 km s^{-1} at 3040 Å.

3.1. The line lists

To compute the synthetic spectrum we adopted as main line list the file gfall05jun16.dat, available on the Kurucz website on June 2016 (Kurucz 2016, K16)[2]. All the lines arising from observed levels of elements from hydrogen to zinc up to six or more ionization degrees are listed with wavelength, log gf value, excitation potential of upper and lower levels and broadening parameters. The log gf values are taken from the literature, mostly when experimental data are available, otherwise the values are those computed by Kurucz with a semi-empirical method.

The list also includes lines of Fe II (Castelli & Kurucz 2010), Fe I (Peterson & Kurucz 2015), and Mn II (Castelli et al. 2015) observed in high-resolution stellar spectra but neither measured or classified in laboratory work. They arise from energy levels predicted (approximately) by the theory. The method takes note of coincidences of unidentified stellar spectral lines with the lines arising from a given predicted energy level. After an appropriate energy shift (correction) of the levels, the lines may be considered to be identified, and used in spectral synthesis.

For elements heavier than zinc the Kurucz line lists contain lines taken from the literature. They are mostly lines of neutral and first ionized atoms.

We changed and implemented the line data in the Kurucz line list. The big file gfall05jun16.dat was divided into several smaller files that we then modified. The main changes were made on Cr II, Cr III, Mn II, Mn III, and Fe II. For numerous lines of Cr II and Fe II, the Kurucz log gf values were replaced by those given in the Fe II and Cr II line lists from Raassen & Uylings (1998), which were available some time ago on a website cited by the authors, but it is no longer online. We changed a log gf value from Kurucz only when that from Raassen & Uylings (1998) improved the agreement between the observed and computed spectra. For a few Cr III lines and several Mn II and Mn III lines we lowered the Kurucz log gf value when it gave rise to a very strong computed, but unobserved line. We checked these changes by comparing synthetic spectra of the HgMn star HD 175640 and of the normal star ι Her with their STIS spectra.

For other elements we modified the Kurucz line lists by using data taken from the atomic database (version 5)[3] (Kramida et al. 2015) of the National Institute of Standards and Technology (NIST), or from more recent literature. We both modified several log gf values and added lines for Ga I, Ga II, Ge II, Zr II, Ru II, Rh II, Pd II, Ag II, Cd II, Sn II, Os II, Ir II, Hg I, and Hg II. For In II we only replaced by the NIST values the atomic data of the Kurucz line list for the 1250−3000 Å region. We added lines of Ga III, As II, Y III, Zr III, Xe I, Xe II, Yb III, Pt II, Pt III, Au II, Au III, Hg III, and Tl II. At the moment these ions are left out of the Kurucz line list. References for the modified or added log gf sources of the ions relevant for this paper are given in Table 1. The complete modified list may be obtained at the Castelli's website[4].

3.2. The abundances

A short description of the elements observed in the ultraviolet spectrum of HR 6000 together with a list of the analyzed lines with the atomic data and the corresponding abundances is given in Appendix A. The average abundance for each element is given in Col. 6 of Table 2, which also displays in successive columns the abundances for HR 6000 determined from spectra observed with different instruments in different ranges and by different researchers, as described in the Introduction. Column 2 of Table 2 lists the abundances derived from the IUE spectra by Castelli et al. (1985, CCHM85) and Col. 3 those obtained from IUE spectra by Smith & Dworetsky (1993, SD) and Smith (1993; 1994; 1997, S). Columns 4 and 5 list the abundances derived from the optical spectra by Catanzaro et al. (2004, CLD04) and by Castelli et al. (2009, CKH). In Col. 6 the abundances obtained in this paper from the STIS spectrum are given (CCACL16). The final abundances from both UVES and STIS spectra are collected in Col. 7. Columns 8 and 9 list the solar abundances from Asplund et al. (2009), Scott et al. (2015a,b), and Grevesse et al. (2015) and their differences with the HR 6000 abundances. Advancing from Cols. 2 to 7 one can note the increasing number of elements for which abundances became available with time and the decreasing number of upper limits.

[2] http://kurucz.harvard.edu/linelists/gfnew/

[3] https://www.nist.gov/PhysRefData/ASD/lines-from.html

[4] http://wwwuser.oats.inaf.it/castelli/linelists.html

Table 1. log gf sources for the heavy elements relevant for this paper.

Elem	log gf sources[a]
Ga I	NIST5 (Shirai et al. 2007), K16
Ga II	NIST5 (Shirai et al. 2007), K16, Ryabchikova & Smirnov (1994), Nielsen et al. (2005), HD 175640
Ga III	NIST5 (Shirai et al. 2007), guessed[b] , HD 175640
Ge II	NIST5 (Wiese & Martin 1980), Morton (2000); K16
As II	Biemont et al. (1998)
Y III	Biémont et al. (2011)
Zr II	Ljung et al. (2006), K16
Zr III	NIST5 (Reader & Acquista 1997)
Cd II	NIST5 (Wiese & Martin 1980), K16, guessed[b]
In II	NIST5 Curtis et al. (2000); Jönsson & Andersson (2007); Ansbacher et al. (1986) (see the comment in NIST5)
Sn II	NIST5 (Oliver & Hibbert 2010; Haris et al. 2014; Alonso-Medina et al. 2005)
Xe I	NIST5 (Fuhr & Wiese 1998)
Xe II	Yüce et al. (2011)
Au II	Fivet et al. (2006); Rosberg & Wyart (1997) , Biémont et al. (2007)
Au III	Enzonga Yoca et al. (2008), Wyart et al. (1996)
Hg II	NIST5 (Sansonetti & Reader 2001), Proffitt et al. (1999)
Hg III	Proffitt et al. (1999)

Notes. [(a)] K16: Kurucz (2016); NIST5 is the version 5 of the NIST database (Kramida et al. 2015). In parenthesis are given the original sources quoted in the NIST database. [(b)] Guessed log gf values are estimated values on the basis of laboratory intensities and excitation energies.

In addition to the non-solar abundances for almost all the observed elements, we point out two other types of abundance anomalies as follows:

1. Ionization anomalies, i.e., LTE abundances for some elements that are markedly inconsistent among different ionization states. The most significant abundance differences are pointed out in Table 3.
2. The considerable line-to-line variation in the derived abundances for C I, N I, Al II, Si II, Si III, Cl I, Ti III, Mn III, Sn II, and Au II. The large scatter in the abundances can be inferred from the large mean square error associated with the final average abundance listed in Col. 7 of Table 2 for the considered ion.

In the final spectrum synthesis calculation, it was necessary to adopt single abundances for elements with different abundances for different ionization stages. This is also needed for abundance comparisons with other stars such as in Table 4. For the light and heavy elements we chose the abundances of the dominant ionization state, except for silicon for which we preferred to adopt the value −7.35 dex obtained from the Si II lines at 3862.595, 4128.074, and 4130.894 Å. For the iron-group elements we adopted the abundances derived from the first ionization state, if observed, because the log gf values available for this state are usually more critically evaluated than those for the second ionization degree. The difference of these abundances with respect to the solar values are listed in Col. 3 of Table 4 and are plotted in Fig. 1. Upper limits for Na, Cl, Co, Zn, Ge, Sr, and Zr are indicated with an arrow. The figure shows a tendency for the elements from He to Zr to be more or less depleted relative to the Sun, except for Be, P, Ti,Cr, Mn, Fe, Ga, and Y. Instead, the observed heavy elements with atomic number $Z \geq 50$ are overabundant, in particular Cd, Xe, and Au, which show enhancements from 3 to 4 orders of magnitude.

The adopted abundances were used to compare the chemical composition of HR 6000 with that of other HgMn stars. Ghazaryan & Alecian (2016) presented a compilation of the abundances taken from the most recent literature for a sample of 104 HgMn stars. Table 4 compares the over- and underabundances of HR 6000 with the minimum and maximum abundances of a given element from the Ghazaryan & Alecian (2016) compilation. The table shows that for HR 6000 the most impressive deviation from the abundance peculiarities observed in the other HgMn stars is the underabundance of silicon, followed by the underabundances of cobalt, copper, strontium, and zirconium. We note that the silicon underabundance −1.975 dex and −2.065 dex for the two stars of the HgMn sample from Ghazaryan & Alecian (2016), HD 158704 and HD 35548, are based on the wrong log gf values −0.360 and −1.30 for the two Si II lines at 4028.465 Å and 4035.278 Å, respectively (Hubrig et al. 1999). The updated log gf values −2.322 and −3.238 (Kurucz 2016) increase the silicon underabundance to [0.0] and to [−0.5], respectively. The underabundance of carbon in HR 6000 is at the lower limit of the carbon underabundances given for the sample. The overabundances of phosphorous and iron are at the upper limit of the overabundances of these elements in the sample of HgMn stars, while the overabundance of gallium is slightly below the lower limit of the gallium overabundance in the other HgMn stars. The other elements are all fully included within the abundance ranges spanned by the HgMn stars of the sample.

4. NLTE and stratification

The classical LTE abundance analysis of the ultraviolet spectrum of HR 6000 described in the previous sections has pointed out the presence of numerous abundance anomalies and inhomogeneities. We can therefore state a posteriori that a more refined theory is needed to predict a spectrum that fits the observations better than the spectrum we computed fits. Possible explanations for the observed abundance anomalies can be NLTE-effects and the occurrence of diffusion and vertical abundance stratification.

There are few NLTE studies available for stars in the temperature range from 10000 to 15 000 K and these studies are mostly devoted to investigate lines in the optical and infrared regions. In fact, to explain the Si II−Si III anomaly observed in a set of late B-type stars, Bailey & Landstreet (2013) performed a rather elaborate test to conclude that NLTE-effects in Si could be potentially important well below the conventional limit of $T_{\rm eff}$ = 15 000 K. However, they demonstrate that a vertical abundance stratification of silicon can also partly provide an explanation of the observed silicon anomaly.

Hempel & Holweger (2003) concluded from a NLTE abundance analysis in the optical region of 27 optically bright B5-B9 main-sequence stars that elemental stratification due to diffusion is a common property of these stars.

A NLTE analysis of C I lines at 1657 Å and C II lines at 1334−1335 Å performed by Cugier & Hardorp (1988) for main-sequence stars of spectral types A0 to B3, has shown remarkable NLTE effects on C I lines in π Cet, a star with stellar parameters close to those of HR 6000. The C I lines computed in NLTE are weaker and narrower than the LTE lines, so that a NLTE synthetic spectrum would improve the agreement between observations and computations in the case of HR6000. Instead, NLTE C II lines have a narrower core than the LTE lines, but the difference in the wings is negligible. Therefore NLTE effects do not explain the very broad wings observed in HR 6000. More in general, Cugier & Hardorp (1988) have demonstrated that the resonance lines of C II at 1335 Å are largely insensitive

Table 2. Abundances $\log(N_{\rm elem}/N_{\rm tot})$ in HR 6000 from different studies.

Elem	CCHM85 IUE	S, SD IUE	CLD04 FEROS	CKH UVES	CCACL16 STIS	Final	Sun	HR-Sun
He I[a]			−2.50 ± 0.10	−2.11		−2.11	−1.11	−1.0
Be II[a]	≤−9.5			−9.78		−9.78	−10.66	+0.88
B II[a]	−10.1				−10.1	−10.1	−9.34	−0.76
C I	≥−5.4				−6.1/−4.9	−5.52 ± 0.30	−3.61	−1.91
C II[a]	≥−5.4		≤−5.60 ± 0.10	−5.50	no fit	−5.50		−1.89
N I	≥−6.5:			≤−5.82	−6.8/−5.6	−6.01 ± 0.47	−4.21	−1.80
N II[a]					−5.2	−5.23 ± 0.04		−1.02
O I	−3.3		−3.80 ± 0.10	−3.68 ± 0.4	−3.68	−3.68 ± 0.04	−3.35	−0.33
Ne I[a]				−5.34		−5.34	−4.11	−1.23
Na I			≤−4.64 ± 0.15	≤−5.71		≤−5.71	−5.83	≤+0.12
Mg II	−5.6	−5.3 ± 0.13	−6.00 ± 0.10	−5.66	−5.42 ± 0.05	−5.45 ± 0.09	−4.45	−1.00
Al II[a]	−7.7		≤−6.75 ± 0.11	≤−7.30	−7.8 ± 0.3	−7.8 ± 0.3	−5.61	−2.19
Al III	−7.7				−7.7	−7.7		−2.09
Si II	≤−5.7		≤−7.15 ± 0.37	−7.33 ± 0.26	−8.35/−6.00	−6.99 ± 0.64	−4.53	−2.46
Si III[a]	−4.3, −5.7				−8.35/−6.45	−7.60 ± 0.59		−3.07
Si IV	−5.7:				−6.65	−6.65		−2.12
P I	≤−4.4				−5.53 ± 0.08	−5.53 ± 0.08	−6.63	+1.10
P II[a]	−3.0/−6.5		−4.64 ± 0.23	−4.57 ± 0.10[b]	−4.54 ± 0.11	−4.55 ± 0.10		+2.08
P II[a]				−4.32 ± 0.09[c]		−4.32 ± 0.09		+2.31
P III	−5.0			−4.69 ± 0.09	≤−5.22 ± 0.32	−4.76 ± 0.14		+1.87
S II[a]	−5.5		≤−5.85 ± 0.10	−6.36	−6.17 ± 0.23	−6.36	−4.92	−1.44
Cl I	−3.3/−6.3			≤−7.74		≤−7.74	−6.54	≤−1.20
Ca II	−5.2			−5.68	−5.70 ± 0.09	−5.70 ± 0.09	−5.72	−0.02
Sc II	≤−11.0		≤−9.15 ± 0.10	≤−9.50				
Sc III[a]					−10.0 ± 0.28	−10.0 ± 0.28	−8.88	−1.12
Ti II	−6.0		−6.56 ± 0.10	−6.47 ± 0.13		−6.47 ± 0.13	−7.11	+0.64
Ti III[a]	−5.8/−6.5				−6.37 ± 0.41	−6.37 ± 0.41		+0.74
V II	≤−6.7			≤−9.2	−9.23 ± 0.12	−9.23 ± 0.12	−8.15	−1.08
Cr II	−6.2	−6.4 ± 0.4	−6.25 ± 0.08	−6.1 ± 0.09	−5.9 ± 0.2	−6.10 ± 0.25	−6.42	+0.32
Cr III[a]	−5.2/−6.2				−6.22 ± -0.25	−6.22 ± 0.25		+0.20
Mn II	−5.3/−6.3	−5.3 ± 0.1	−5.6 ± 0.10	−5.18 ± 0.32	−5.29 ± 0.21	−5.29 ± 0.21	−6.62	+1.33
Mn III[a]	−5.3:				−5.79 ± 0.36	−5.79 ± 0.36		+0.83
Fe I			−3.95 ± 0.03	−3.65 ± 0.07		−3.65 ± 0.07	−4.57	+0.92
Fe II	−3.91 ± 0.27	−3.7 ± 0.05	−3.98 ± 0.20	−3.65 ± 0.09	−3.68 ± 0.05	−3.65 ± 0.09		+0.92
Fe III[a]	−3.73 ± 0.42		−3.86 ± 0.20		−3.78 ± 0.14	−3.78 ± 0.14		+0.79
Co II[a]	≥−9.3	≤−9.0		≤−8.42	≤−10.12	≤−10.12	−7.11	≤−3.01
Ni II[a]	−5.5/−7.0	−6.3 ± 0.2	≤−6.00 ± 0.10	−6.24	−6.24	−6.24	−5.84	−0.40
Ni III	−6.5/−7.0				−6.64 ± 0.14	−6.64 ± 0.14		−0.80
Cu II[a]	≥−9.3	−7.5	−10.53	≤−7.83	−10.53	−10.53	−7.86	−2.67
Zn II[a]	−8.3	−9.2			≤−8.84	≤−8.84	−7.48	≤−1.36
Ga II[a]	−8.4				−8.85	−8.85	−9.02	+0.36
Ga III					−8.15	−8.15		+0.86
Ge II					≤−10.64	≤−10.64	−8.41	≤−2.23
As II[a]					−9.74	−9.74	−9.74	0.0
Sr II				≤−10.67		≤−10.7	−9.21	≤−1.49
Y II				−8.60		−8.60	−9.83	+1.23
Y III[a]					−7.6	−7.6		+2.23
Zr III[a]					≤−10.24	≤−10.24	−9.45	≤−0.79
Cd II[a]					−7.00	−7.00	−10.27	+3.27
In II[a]					−10.24:	−10.24:	−11.24	+1.00
Sn II					−8.23 ± 0.64	−8.23 ± 0.64	−10.02	+1.79
Xe I					−5.55 ± 0.45	−5.55 ± 0.25	−9.80	+4.25
Xe II[a]				−5.25 ± 0.17		−5.25 ± 0.17		+4.55
Au II[a]					−7.82 ± 0.55	−7.82 ± 0.55	−11.13	+3.31
Au III					−8.80 ± 0.28	−8.80 ± 0.28		+2.33
Hg II[a]	–	−9.25/−7.25	≤−8.00 ± 0.10	−8.20	−9.60	−9.60	−10.87	+1.27

Notes. [(a)] Dominant ionization state. [(b)] Average P II abundance with lines with λ within 4044 Å and 5200 Å. [(c)] Average P II abundance with lines with $\lambda \geq 5200$ Å.

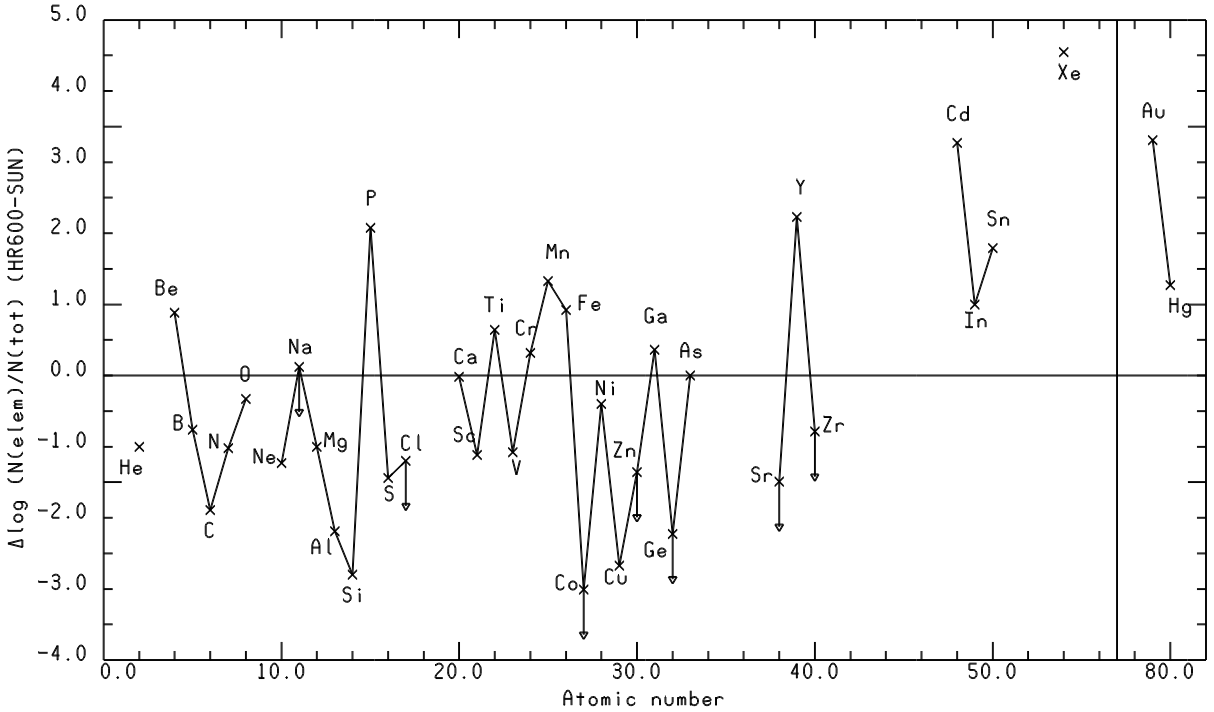

Fig. 1. Differences between the abundance from a selected ion of a given element in HR 6000 and the solar abundance, as they are listed in Col. 3 of Table 4. The arrow for Na, Cl, Co, Zn, Ge, Sr, and Zr indicates an upper abundance limit. The vertical full line indicates the jump from $Z = 57$ to $Z = 77$, a range in atomic numbers for which no elements were observed in HR 6000. The errors can be inferred from Col. 1 of Table 4.

Table 3. Elements with strong ionization abundance anomalies.

Ion1	Ion2	log ϵ1–log ϵ2
N I	N II	−0.88
Si II	Si III	+0.60
Si III	Si IV	−1.00
P I	P II	−1.08
Mn II	Mn III	+0.50
Ga II	Ga III	−0.65
Y II	Y III	−1.00
Au II	Au III	−0.98

to effective temperature, microturbulence, and NLTE effects in late B-type stars.

Given the difficulty of discussing NLTE-effects in HR 6000 owing to the scarce sources available in the literaure for star of this spectral type, and because we do not have the tools to carry out non-LTE synthesis for this study, we consider here the hypothesis of vertical abundance stratification in more detail. We hope that this paper encourages investigators to perform studies on the NLTE effects on ultraviolet lines in HgMn and related stars.

Ryabchikova et al. (2003) discuss spectroscopic observational evidence for the vertical abundance stratification in stellar atmospheres. In HR 6000 all these observational signs are present, and in particular, we find:

1. The impossibility to fit the wings and core of strong spectral lines with the same abundance. It was observed for He I in the optical region (Castelli & Hubrig 2007), for C I and for the strong C II and Si II lines in the ultraviolet.
2. Violation of LTE ionization balance. This occurs in HR 6000 for N I, N II, Si II, Si III, Si IV, P I, P II, Mn II, Mn III, Ga II, Ga III, Y II, Y III, and Au II, Au III (Table 3).
3. Disagreement between the abundances derived from strong and weak lines of the same ion. In traditional atmospheric analysis, this trend is eliminated by introducing microturbulence. In the present case, abundances are typically lower for the strongest lines. This cannot be changed by taking a lower microturbulence, as we have already adopted a microturbulence of zero. The effect is present for all the elements with average abundances affected by a large mean square error. They are C I, N I, Si II, Si III, Cl I, Ti III, Mn III, Sn II, and Au II (Table 2).
4. An unexpected behavior of high-excitation lines of the ionized iron peak elements. For $\lambda > 5800$ Å, emission lines were observed in HR 6000 for Cr II, Mn II, and Fe II (Castelli & Hubrig 2007). Sigut (2001) showed that NLTE effects coupled with a stratified manganese abundance satisfactorily accounts for the emissions from the Mn II lines at $\lambda\lambda$ 6122–6132 Å observed in several HgMn stars, HR 6000 included.
5. Different abundances obtained from different lines of the same ion formed at a priori different optical depths, for example, before and after the Balmer jump, in the UV and visual spectral region. In addition to the possibility of different abundances for mercury, as discussed above, this anomaly was observed for Mg II. The ultraviolet lines are consistent with the abundance of -5.45 ± 0.09 dex, while the doublet at 4481 Å indicates an abundance of −5.7 dex.

Stratification may manifest itself in one or more of the ways enumerated. We call attention to cases where stratification is indicated by the profile of a single line (Item 1) or several lines (Items 2–5). Stratification is indicated by the line profiles in only a few cases. The various indicators may overlap in a given element (Silicon) or spectrum (Si II).

We searched in more detail the presence of stratification for carbon, nitrogen, silicon, phosphorous, manganese, and gold.

Table 4. Adopted abundances compared with solar values, as well as with extreme (maximum and minimum) values for stars from the Ghazaryan & Alecian (2016) compilation.

Element	HR 6000	HR 6000-Sun	Lower limit	Star	Upper limit	Star	Number of stars
He I	−2.11	−1.00	−1.55 ± 0.13	HR 2676	+0.79 ± 0.12	Platais 1 No1	64
Be II	−9.78	+0.88	−0.135	HD 71066	+0.015	HD 175640	2
B II	−10.1	−0.76	−2.48	χLupi	−2.48	χLupi	1
C II	−5.50	−1.89	−1.79	112 Her A	+0.47 ± 0.05	HR 8118	49
N II	−5.23 ± 0.04	−1.02	−2.265 ± 0.35	νHer	+0.47	21 Aql	14
O I	−3.68 ± 0.04	−0.33	−0.4	HR 8118; 46 Dra A	+0.72	HR 8349	35
Ne I	−5.34	−1.23	−1.4	ν Her	+0.69	κCnc A	27
Na I	≤−5.71	≤+0.12	+0.285 ± 0.09	HD 71066	+0.865	HR 7775	6
Mg II	−5.45 ± 0.09	−1.00	−1.76	HD 55362	+0.30 ± 0.25	HR 2844	67
Al II	−7.8 ± 0.3	−2.19	−2.75 ± 0.37	112 Her A	+0.39	HD 173673	43
Si II	−7.33 ± 0.26	−2.80	−1.49 ± 0.03	HD 55362	+0.355	HR 7775	71
P II	−4.55 ± 0.10	+2.08	+0.14	53 Tau	+2.235	74 Aqr A	38
S II	−6.36	−1.44	−1.94 ± 0.51	HD 55362	+0.47 ± 0.25	HR 7018	51
Cl I	≤−7.74	≤−1.20	−1.40	χLupi A	−0.36	HD 46866	2
Ca II	−5.70 ± 0.09	−0.02	−0.805 ± 0.21	HD 71066	+1.215	HD 158704	53
Sc III	−10 ± 0.28	−1.12	−1.90	ϕPhe	+1.83	HR 8118	37
Ti II	−6.47 ± 0.13	+0.64	−0.34 ± 0.15	21 Aql	+1.465	1 Cen	60
V II	−9.23 ± 0.12	−1.08	−1.895	HD 71066	+1.155	μ Lep	14
Cr II	−6.10 ± 0.25	+0.32	−1.44 ± 0.2	46 Aql	+1.20 ± 0.26	ϕ Her A	86
Mn II	−5.29 ± 0.21	+1.33	−0.23 ± 0.16	36 Lyn	+2.87 ± 0.40	BD 0984	67
Fe II	−3.65 ± 0.09	+0.92	−1.10 ± 0.20	87 Psc	+0.92	112 Her A	84
Co II	≤−10.12	≤−3.01	−2.49	several	+2.945	ιCrB A	29
Ni II	−6.24	−0.40	−2.085	HD 71066	+0.66 ± 0.13	HD 49886	49
Cu II	−10.53	−2.67	−0.89 ± 0.36	12 Her A	+2.21 ± 0.15	HR 7361	28
Zn II	≤−8.84	≤−1.36	−2.56	ϕPhe	+1.86	ϕHer A	30
Ga II	−8.66	+0.36	+0.81 ± 0.30	46 Aql	+4.21	αAnd	35
Ge II	≤−10.64	≤−2.23	−1.65	χLupi A	−1.65	χLupi A	1
As II	−9.74	0.00	+2.33	χLupi A	+3.365	HD 71066	2
Sr II	≤−10.7	≤−1.49	−1.17	112 Her A	+2.940	HR 7775	44
Y III	−7.60	+2.23	+0.67	HR 2676	+4.3	HD 2844	53
Zr III	≤−10.24	≤−0.79	+4.95 ± 0.15	HR 7775	+2.85	AV Scl	34
Cd II	−7.00	+3.27	+0.56	χLupi A	+0.56	χLupi A	1
In II	−10.24	+1.00	−−	−−	−−	−−	0
Sn II	−8.23 ± 0.64	+1.79	+1.38	χLupi A	+1.38	χLupi A	1
Xe II	−5.25 ± 0.17	+4.55	+2.98 ± 0.11	ϕHer A	+4.89 ± 0.14	κCnc A	29
Au II	−7.82 ± 0.55	+3.31	+3.5	46 Dra A	+5.74	66 Eri B	11
Hg II	−9.60	+1.27	+1.06	53 Tau	+6.61 ± 0.20	USNO-A2.0 0825-03036752	82

The lines of gallium have oscillator strengths that are too uncertain to be used, while yttrium has too few lines, none of which have wings.

We determined the atmospheric layers where the optical depth of several points of a given profile from the center to the wings is $\tau_\nu = 1$. Each profile was computed with the WIDTH code (Kurucz 2005) for the particular abundance determined from that line using the synthetic spectrum (Table A.1). Among the several outputs of the WIDTH code there is the mass depth value (ρx) of the layer where $\tau_\nu = 1$ for each of the considered line profile points, as well as the average mass depth of the forming region of the line, defined as

$$\log_{10}(\rho x)_{av} = \frac{\int_0^b \log_{10}(\rho x)_{\tau\nu=1}(1 - H_\nu(0)/H_c(0))\mathrm{d}\nu}{\int_0^b (1 - H_\nu(0)/H_c(0))\mathrm{d}\nu}$$

where the integral is performed over the frequencies from center to wings and $H_\nu(0)$ and $H_c(0)$ are the line and continuum Eddington flux at the stellar surface, respectively. For more details see Castelli (2005).

As further step, in order to be consistent with other papers dealing with stratification, the mass depth scale (ρx) was converted to the continuum optical depth scale at $\lambda = 5000$ Å (τ_{5000}). Finally, the abundance derived with the synthetic spectrum from each line was plotted as a function of $\log(\tau_{5000})_{\rm aver}$, the average optical depth of line formation. Figures 2a, 4a, 7a, 9, 10a, and 12a show these plots for carbon, nitrogen, silicon, phosphorous, manganese, and gold.

This kind of approach, which is an indication of the presence of stratification for a given element, is similar to that used in others studies on this subject, although usually the optical depth in the line core is considered (Khalack et al. 2007, 2008; Thiam et al. 2010) rather than the average optical depth adopted here. Qualitatively, we expect that stronger lines are formed higher in the photosphere than weaker lines. Since the current study is based on synthesis rather than equivalent widths, we use depth τ_{5000} where the line profile optical depth is unity as a proxy for the line strength.

We carried out a series of simple experiments for some elements. We derived, by means of trial and error, an empirical

step-like function of abundance versus log(τ_{5000}) for a given element. The adopted functions reduce the observed abundance anomalies when used in the synthetic spectrum computations. This basic approach is used for both anomalous line profiles and sets of lines with inconsistent abundances from the unstratified model. We do not claim that these functions are unique. In fact, only a more rigorous theoretical approach including the stratification on the temperature-pressure structure of the atmosphere could give an adequate answer concerning the origin of the observed abundances inhomogeneities.

Empirical step functions for the abundance of carbon, nitrogen, silicon, manganese, and gold are given in Figs. 2b, 4b, 7b, 10b, and 12b. These elements are now discussed.

4.1. Carbon

Several signs of possible vertical abundance stratification are present for carbon. Numerous C I lines can be observed in the ultraviolet, but most of them have profiles that cannot be reproduced by an unique abundance. In fact, they have an observed core that is too weak as compared to that of the computed profile whose wings fit the observed spectrum. The best fit abundance from C I individual lines ranges from −6.1 dex to −4.9 dex. The average abundance is −5.52 ± 0.3 dex, which is consistent with the value −5.50 dex derived by Castelli et al. (2009) from the C II lines at 4267.001 Å and 4267.261 Å. However, a plot of the C I abundance versus log τ_{5000}(aver) does not shows any dependence of the abundance on the optical depth (Fig. 2a).

For C II, it is impossible to reproduce the resonance profile at $\lambda\lambda$ 1335.663, 1335.708 Å, with any abundance that is constant with depth. Either the core is fitted but not the wings or the wings are fitted but not the core. The same kind of anomaly affects the strong C II profile at 1323.9 Å. We note that the C II line at 1334.532 Å cannot be used for the abundance analysis because it is blended with a strong blue component of interstellar or circumstellar origin.

We were able to fit, at the same time, both the core and wings of C II at 1335.663, 1335.708 Å with the carbon abundance profile, shown in Fig. 2b, obtained with trial and error.

In Fig. 3 the C I and C II lines computed with both the average carbon abundance −5.5 dex and the abundance step function shown in Fig. 2b are plotted. They are compared with each other and with the observed spectrum. We point out that while the step function improves the agreement between the observed and computed spectra, as shown in Fig. 3, some non-negligible inconsistencies are still present. In particular, the C II line at 1323.9 Å is still poorly reproduced. As already discussed at the beginning of Sect. 4, we would like to stress that a NLTE analysis could clarify whether the C I anomalies are related with NLTE rather than a vertical abundance stratification.

4.2. Nitrogen

From the absence of N I lines at 8680.282 Å and 8683.403 Å, Castelli et al. (2009) determined an upper limit of −5.82 dex ([−1.7]) for the nitrogen abundance. In the ultraviolet, the N I lines at 1411.9 Å (UV mul.10), 1310.5,1310.9 Å (UV mult. 13), and 1492.625, 1492.820, and 1494.675 Å (mult. 4) are clearly observable, as well as the lines of N II at $\lambda\lambda$ 1275.038, 1275.251 Å and the blend at $\lambda\lambda$ 1276.201, 1276.225 Å. These lines are not all fitted by the same abundance. In fact, the nitrogen abundance is affected by both an ionization anomaly and line-to-line variations: while −5.2 dex reproduces the N II lines, lower values, ranging from −5.9 dex to −6.8 dex, are required to fit the N I lines. The nitrogen abundance versus log τ_{5000}(aver) is shown in Fig. 4a. A steep dependence of the abundance on the optical depth is evident. The abundance inconsistencies decrease if the abundance profile shown in Fig. 4b is used. We obtained this profile from al the N I and N II lines with the trial and error.

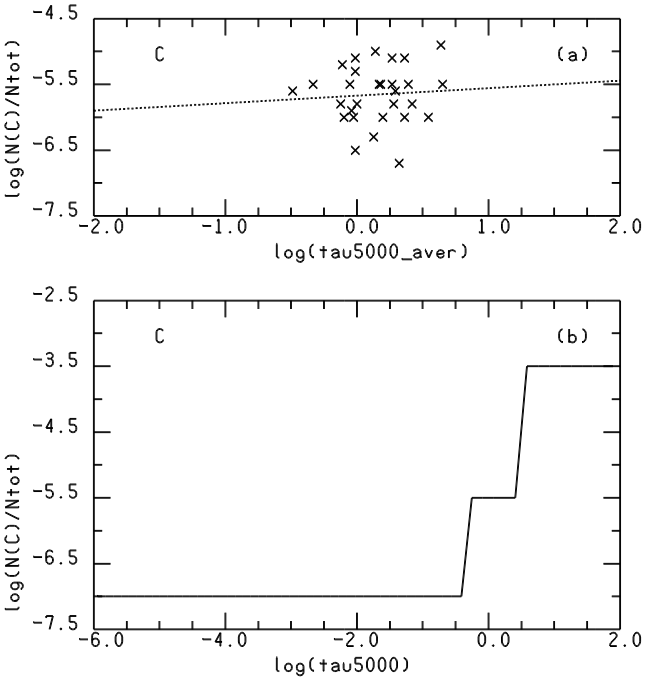

Fig. 2. a) C I abundance versus log τ_{5000}(aver), average depth of line formation on the log τ_{5000} scale. The dashed line is the best fit straight line to the plotted points. **b)** Vertical abundance distribution as function of log τ_{5000} obtained by the trial and error applied to C II $\lambda\lambda$ 1335.663, 1335.708 Å.

The N I and N II lines computed both with a constant abundance −5.23 dex derived from the N II lines and with the abundance step profile shown in Fig. 4b, are compared and with the observed spectrum in Figs. 5 and 6, respectively. The effect of a depth-dependent abundance is large for the N I lines, while it does not affect the observed N II lines.

We note that nitrogen is predominantly singly ionized in late B-star atmospheres, so that the analysis of N I could be particularly susceptible to NLTE effects in the ionization equilibrium. For N I as well as for C I a NLTE analysis is required to state the degree of reliability of the hypothesis of vertical abundance stratification for this element.

4.3. Silicon

A unique silicon abundance cannot be determined from the analysis of several silicon lines present such as Si II, Si III, and Si IV in the ultraviolet spectrum of HR 6000. In fact, the silicon abundance ranges from −8.35 dex to −6.0 dex. All the lines analyzed are collected in Table A.1.

A plot of the silicon abundance versus log τ_{5000}(aver) shows a dependence of the abundance on the optical depth, with upper layers more depleted than the deeper layers (Fig. 7a).

A further significant illustration of the probable silicon stratification in HR 6000 is given by the Si II lines at 1264.738 Å and 1265.002 Å which show a core that is consistent with an

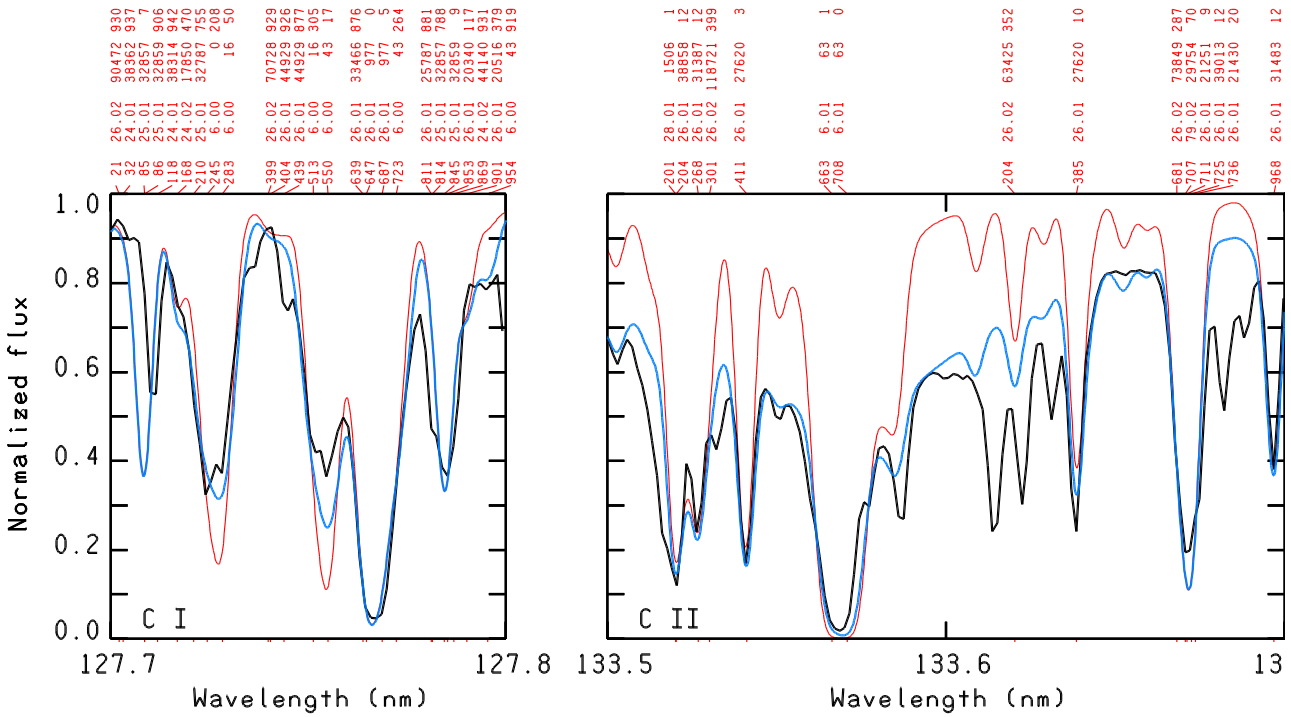

Fig. 3. C I lines of UV mult. 7 ($\lambda\lambda$ 1277.245, 1277.283, 1277.513, 1277.550, 1277.273, and 1277.954 Å) and the C II blend at $\lambda\lambda$ 1335.663, 1335.708 Å computed with both the average carbon abundances of −5.5 dex (red line) and the abundance step function shown in Fig. 2b (blue line) are compared each with other and with the observed spectrum (black line).

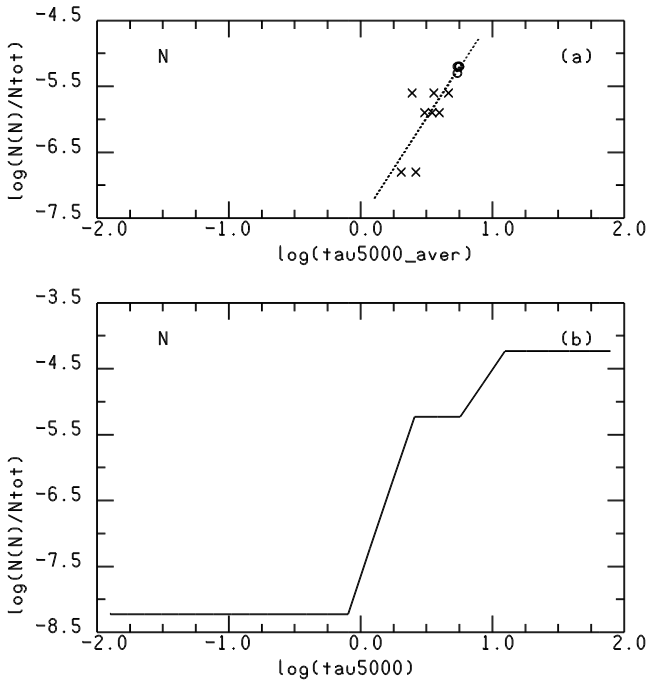

Fig. 4. a) Nitrogen abundance versus log τ_{5000}(aver); crosses are for N I, circles for N II. The dashed line is the best fit straight line to the plotted points. **b)** Vertical abundance distribution as a function of log τ_{5000} obtained by trial and error.

abundance of −8.35 dex and wings consistent with an abundance of −6.65 dex (Fig. 8). This Si II line was used to derive, by means of trial and error, the empirical stratification step profile given in Fig. 7b. Its use in the spectral synthesis allows us to fit numerous Si I and Si II lines simultaneously.

The Alecian & Stift (2010) computations of diffusion of silicon in HgMn stars predict a stratification profile with a maximum underabundance between −0.75 dex and −2.0 dex for $T_{\rm eff}$ between 14 000 K and 12 000 K, and log g = 4. It occurs at log τ_{5000} = −2.0. The empirical stratification profile shown in Fig. 7b implies a silicon abundance that is much lower in the whole atmosphere than that predicted by Alecian & Stift (2010).

4.4. Phosphorous

There are numerous lines of P I, P II, and P III in the spectrum of HR 6000, but they are all more or less blended in the ultraviolet, except for P I at 2136.182 Å, and 2149.142 Å and P II at 2285.105 Å and 2497.372 Å. We used NIST log gf values for most P I lines and for the P II lines of UV multiplet 2 at 1301−1310 Å. For the remaining P I, P II, and P III lines we adopted log gf values from the Kurucz (2016) database. For P II, they do not differ more than 0.01 dex from the NIST values and cover a larger number of lines than the NIST database does.

The average abundances from the P I and P II ultraviolet lines are −5.53 ± 0.08 dex and −4.54 ± 0.11 dex, respectively, so that they differ by 1.0 dex. Because all the ultraviolet P III lines are blended, the P III average abundance is rather uncertain. We assumed an upper limit of $\log(N_{\rm P\,III}/N_{\rm tot}) \le -5.22 \pm 0.32$ dex.

Castelli & Hubrig (2007) did not observe P I lines in the UVES spectrum, while several P II and P III unblended lines were measured. The observed cores of the strong P II lines of multiplet 5 at $\lambda\lambda$ 6024, 6034, and 6043 Å were so deep that they could not be fitted by the computations for any abundance. In this paper, we determined two average abundances from the optical P II lines depending on whether they lie shortward or longward of 5200 Å. These average abundances are −4.57 ± 0.1 dex and −4.32 ± 0.09 dex, respectively. The average abundance from the

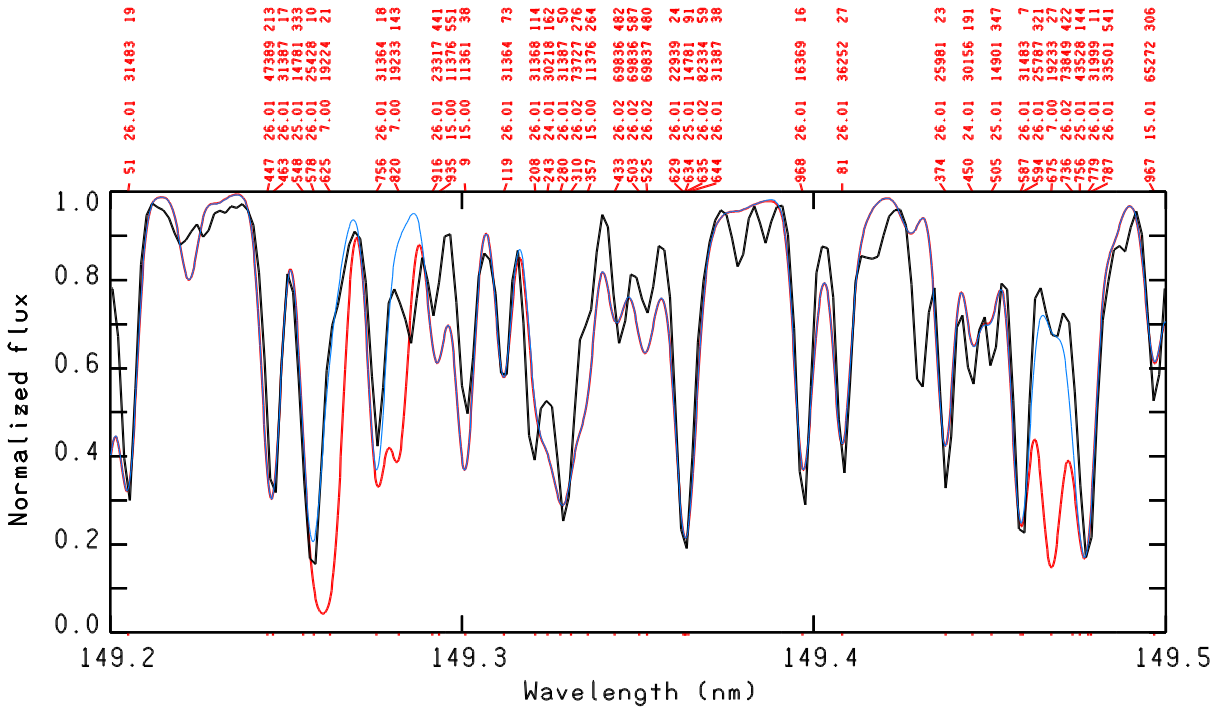

Fig. 5. N I lines of UV mult. 4 at $\lambda\lambda$ 1492.625, 1492.820, and 1494.675 Å computed both with the constant nitrogen abundance −5.23 dex (red line) and with the abundance step function shown in Fig. 4b (blue line). The computed spectra are superimposed to the observed spectrum. The effect of the two different adopted abundances (constant or variable) is evident.

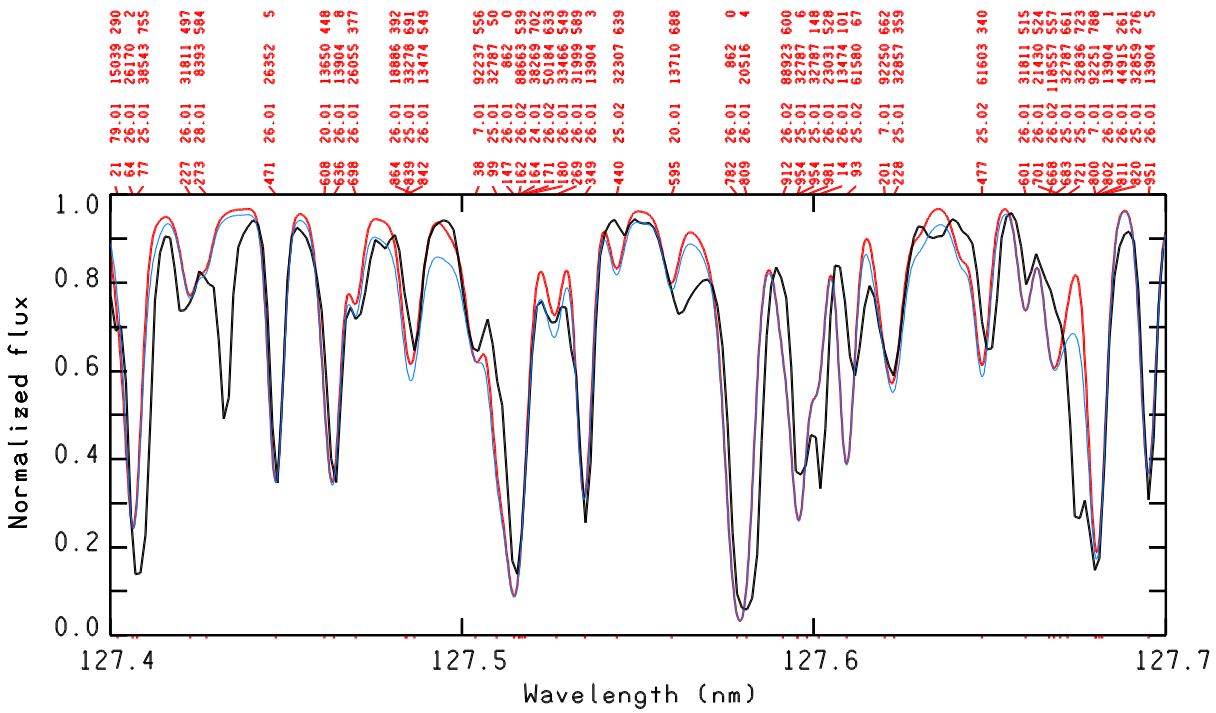

Fig. 6. N II lines at $\lambda\lambda$ 1275.038, 1275.251, 1276.201, and 1276.225 Å computed both with the constant nitrogen abundance −5.23 dex (red line) and with the abundance step function shown in Fig. 4b (blue line). Only the lines at 1275.038 Å and 1276.201 Å are predicted. The computed spectra are superimposed to the observed spectrum. The effect of the two different adopted abundances (constant or variable) is negligible.

optical P III lines is −4.69 ± 0.09. Table 2 summarizes all the above abundance values.

The difference of 1.0 dex, or even larger, between P I and P II abundances and the increasing of the P II abundance from about −4.65 dex at 4000 Å to about −4.3 dex at 6000 Å, led us to search for the presence of vertical abundance stratification for phosphorous.

In Fig. 9, the P I, P II, and P III abundances derived from both ultraviolet and optical lines listed in Table A.1 are plotted as a function of $\log(\tau_{5000})$(aver). While there is a weak dependence on depth for P II (circles), no dependence is present for P I

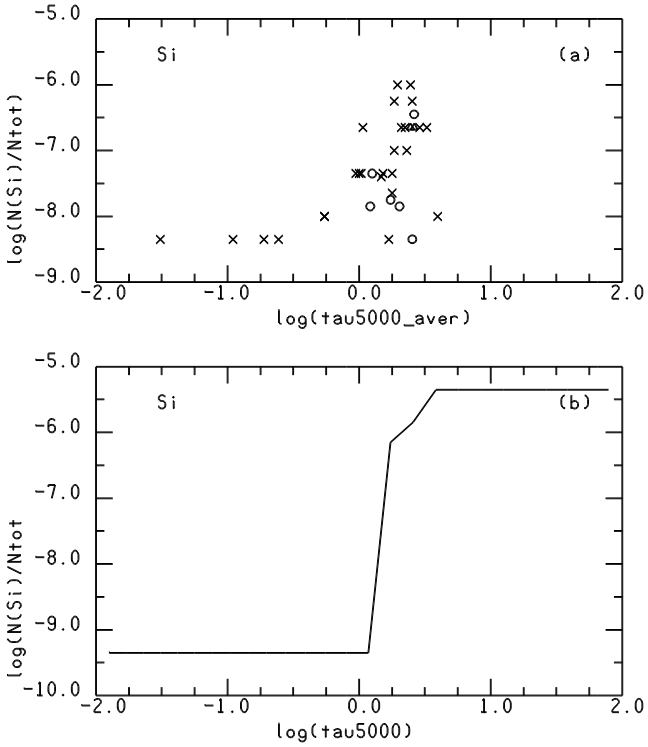

Fig. 7. a) Silicon abundance versus log τ_{5000}(aver); crosses are for Si II, circles for Si III, triangles forSi IV. **b)** Vertical abundance distribution as a function of log τ_{5000} obtained by trial and error.

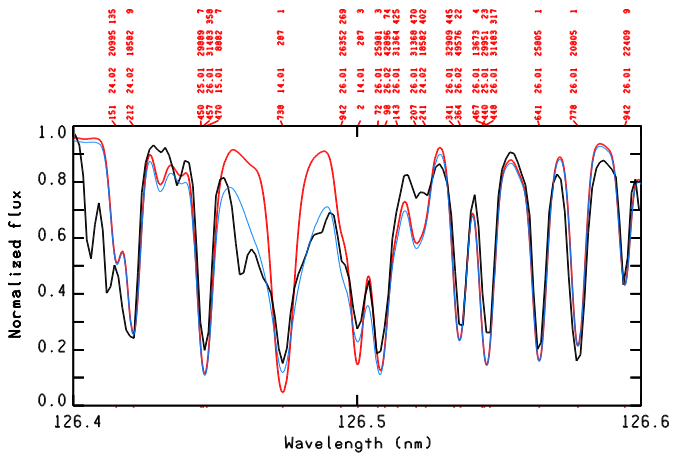

Fig. 8. Si II lines at 1264.738 Å and 1265.002 Å computed with the average silicon abundance −7.35 dex (red line) and the abundance step function of Fig. 7b (blue line). The computed spectra are superimposed on the observed spectrum (black line).

(crosses), which seems to have been formed at the same layers as P II and P III, in spite of the abundance difference of 1 dex. We may speculate that a NLTE analysis of P I would explain the large departure from the ionization equilibrium observed for phosphorous.

4.5. Manganese

The spectrum of HR 6000 is very rich with Mn II and Mn III lines. The manganese abundance of −5.3 dex was obtained from the three Mn II lines at $\lambda\lambda$ 2576, 2593, and 2605 Å, which were also adopted by Smith & Dworetsky (1993) in their

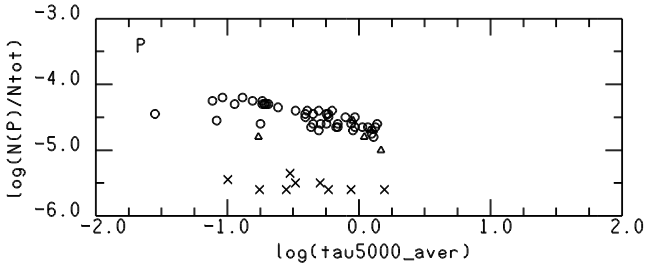

Fig. 9. Phosphorous abundance versus log τ_{5000}(aver); crosses are for P I, circles for P II, triangles for P III.

abundances analysis of HgMn stars from IUE spectra. For HR 6000, we find the same abundance as Smith & Dworetsky (1993).

Although the average abundance −5.29 ± 0.21 dex reproduces almost all the lines examined, there are a few strong Mn II lines with a computed core that is less deep than the observed core. They are indicated with the note "core" in the last column of Table A.1. Most Mn II lines are affected by hyperfine structure. When hyperfine structure was taken into account in the computations a note "hfs" was added in the last column of Table A.1. To compute the hyperfine components we used the hyperfine constants measured by Holt et al. (1999) and by Townley-Smith et al. (2016).

In order to find a good sample of Mn III lines, we examined the lines with log gf values computed by Uylings & Raassen (1997) and extracted the isolated lines and the main components of blends from them (Table A.1). The difference between the log gf values from Uylings & Raassen (1997) and those computed by Kurucz (2016) are on the order of 0.05 dex, except for two lines at 1283.589 Å and 1287.584 Å for which the difference is 0.13 dex. The Mn III abundance equal to −5.79 ± 0.36 dex was derived using the Kurucz log gf values. Their general agreement with those from Uylings & Raassen (1997) supports the finding of 0.5 dex lower Mn III abundance compared to the Mn II value.

Figure 10a shows the Mn II and Mn III abundances versus log τ_{5000}(aver). A dependence of the Mn III abundance (circles) on the optical depth is manifest, while the Mn II abundance (crosses) is constant with depth. However, the abundance adopted for the strong lines did not fit the line center. An increase of abundance or microturbulent velocity increases the wings rather than the line core.

The Alecian & Stift (2010) computations of the diffusion in HgMn stars predict for manganese a stratification profile with a behavior similar to that we derived for HR 6000, but for an overabundance about 2.5 dex larger. Figure 10b compares the vertical abundance distribution as a function of log τ_{5000} obtained by trial and error with that from Alecian & Stift (2010), both in the original form and shifted by −2.5 dex in abundance.

Figure 11 is an example of the better agreement between the observed and computed core achieved for a strong Mn II line when the abundance step function is used in the computations.

4.6. Gold

There is a discrepancy of 1.0 dex between the gold abundance derived from the Au II and Au III lines.

Several Au II lines can be observed in the spectrum of HR 6000, but only few of them are unblended, in particular the Au II lines at 1740.475, 1800.579, 2000.792, and 2082.074 Å. The abundance from the line at 1800 Å is so high compared to

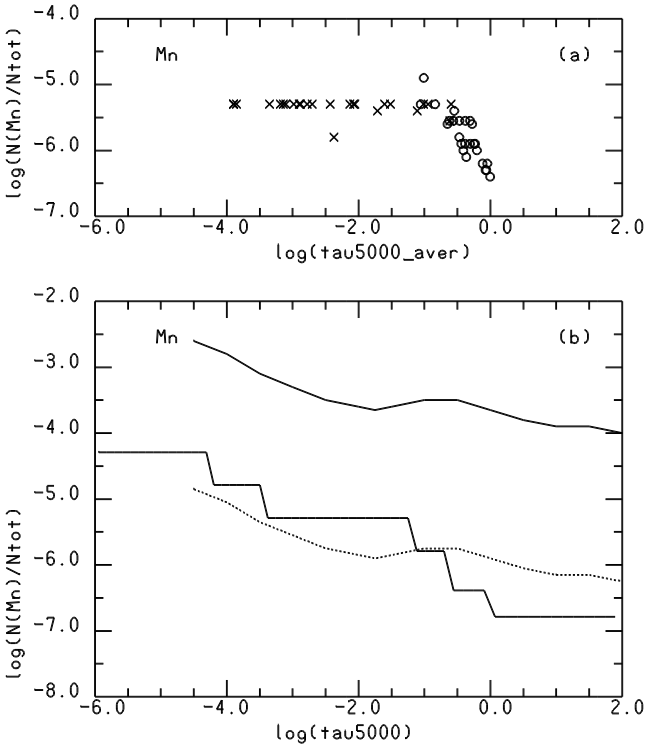

Fig. 10. a) Manganese abundance versus log $\tau_{5000}(aver)$; crosses are for Mn II, circles for Mn III. **b)** Vertical abundance distribution as a function of log τ_{5000} obtained by trial and error. The theoretical vertical stratification for $T_{\rm eff}$ = 14 000 K, log g = 4.0 from Alecian & Stift (2010) is overplotted (full continous line). The dashed line is the same curve shifted by −2.25 dex in the abundance.

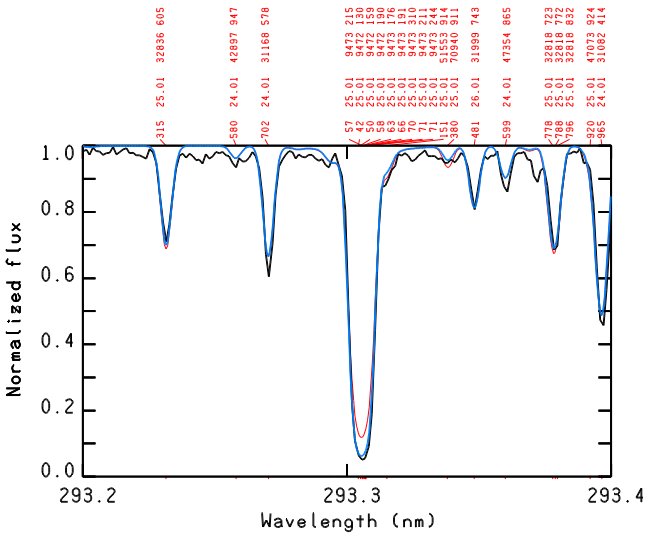

Fig. 11. Mn II line at 2933.054 Å computed with the average manganese abundance −5.29 dex (red line) and the abundance step function of Fig. 10b (blue line). The computed spectra are superimposed on the observed spectrum (black line). The core of the line is well fitted by the abundance step function. The hyperfine structure is considered in the computations.

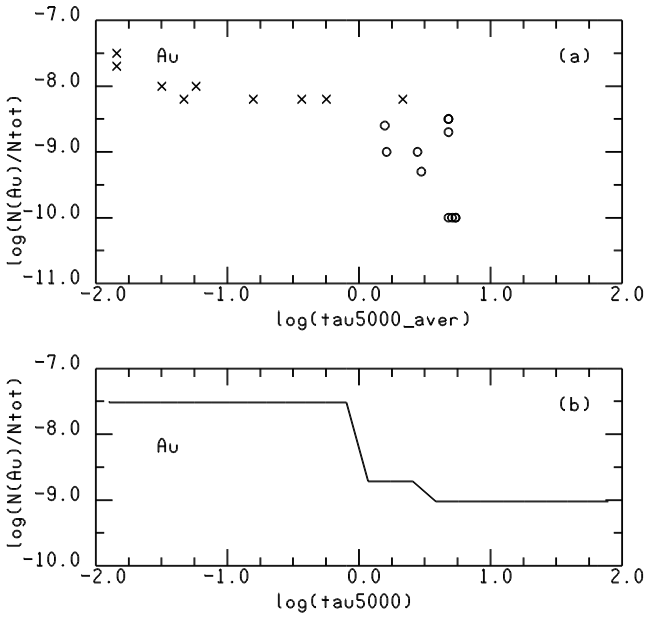

Fig. 12. a) Gold abundance versus log τ_{5000}(aver); crosses are for Au II, circles for Au III. **b)** Vertical abundance distribution as a function of log τ_{5000} obtained by trial and error.

that derived from the other lines that we suspect it is blended with some other unknown component. If we exclude this line, the average abundance from the three unblended lines of Au II is −7.57 ± 0.09 dex. However, the other blended lines are better reproduced by a lower value equal to −8.2 dex. This value also nicely fits the weak unblended line observed at 4052.790 Å in the UVES spectrum. Several Au III lines, mostly blended, are predicted for −8.2 dex, but they are all stronger than the observed lines. The abundance from the Au III lines ranges from −8.5 dex to an upper limit of −10 dex.

We conclude that gold is probably affected by the abundance stratification observed for some other elements as well. Figure 12a shows the Au II and Au III abundances versus log τ_{5000}(aver). The figure shows a dependence of the abundance on the optical depth, with deeper layers more depleted than the upper layers, as for manganese. Figure 12b shows the empirical abundance stratification that we derived from Au II and Au III lines with trial and error. The abundance stratification reduces the gold abundance inhomogeneities observed in the spectrum.

5. Conclusions

This paper has extended to the ultraviolet the abundance analysis of HR 6000 performed by Castelli & Hubrig (2007) and Castelli et al. (2009) on high-resolution spectra in the optical region. In this way we obtained a panoramic view of the spectrum and abundances of all the species observed in this highly anomalous, ultrasharp-lined, non-magnetic, main-sequence, chemically peculiar star.

Thanks to ultraviolet analysis we increased the number of the elements for which abundances can be assigned, because some elements are only observable in the ultraviolet. Also some other elements, which were observed in only one ionization degree in the optical region, are present in more ionization degrees in the ultraviolet. In particular, ions not observed in the visible are: B II, N I, N II, Al II, Al III, Si III, Si IV, P I, Sc III, Ti III, V II, Cr III,

Mn III, Fe III, Ni III, Cu II, Zn II, Ga II, Ga III, Ge II, As II, Y III, Zr III, Cd II, In II, Sn II, Xe I, and Au III.

The comparison of the average abundances of HR 6000 with those of other HgMn stars taken from the Ghazaryan & Alecian (2016) compilation has pointed out the strong underabundance of silicon, already found in other studies, followed by the underabundances determined from Co II, Cu II, Sr II, and Zr III. These elements put HR 6000 outside of the group of HgMn stars according to the abundances collected by Ghazaryan & Alecian (2016). At the lower underabundance limit of the Ghazaryan & Alecian (2016) compilation there is carbon, while phosphorous and iron are at the upper overabundance limit.

We found in this paper that the striking silicon underabundance ([−2.80 ± 0.26]) is not constant with depth, but that vertical abundance stratification accounts for most of the abundance anomalies observed for this element in the ultraviolet. It was modeled with an empirical step function with abundances ranging from −5.35 dex at the bottom of the atmosphere to −9.35 dex at the top of the atmosphere. We examined the possibility of abundance stratification also for some other elements which either do not meet the ionization balance requirement, such as nitrogen, phosphorous, manganese, and gold, or show strong broad profiles that cannot be fitted by an unique abundance, such as C II at $\lambda\lambda$ 1335.663, 1335.708 Å. For all these elements, except for carbon and phosphorous, we found both a dependence of the abundance on the optical depth and an empirical abundance profile, which reduces the disagreement between the observed and computed spectra when it is adopted in the synthetic spectrum computation. For carbon, we found an empirical stratified abundance profile which roughly fits both the core and wings of C II at $\lambda\lambda$ 1335.663, 1335.708 Å, reduces the disagreement between a few observed and computed C I profiles, but still does not explain other discrepancies, in particular that for C II at 1323.9 Å. For phosphorous, we pointed out a weak dependence of the P II abundance on the optical depth, but the presence at the same depths of P I and P II lines with abundances differing by 1 dex, has hampered any determination of some empirical abundance stratification profile.

Other elements could be affected by abundance stratification, such as, for instance, yttrium and gallium, which were not analyzed here because there were too few observed lines or their log gf values were uncertain. There are other elements that do not show any sign of vertical stratification. This is true for iron in spite of its high overabundance.

In this paper we estimated abundance stratification profiles for C , N , Si , Mn , and Au in an empirical way by using the trial and error method. We are aware that a more rigorous approach should be used, taking into account either an empirical abundance stratification on the temperature-pressure structure of the model atmosphere (Nesvacil et al. 2013) or including the diffusion velocities in the model atmosphere computations (Alecian & Stift 2010; Stift & Alecian 2012). Last but not least, NLTE effects on the HR 6000 abundances should be investigated. We note that while numerous NLTE analyses were performed for stars hotter than 15 000 K and stars cooler than 10 000 K, very few and sparse work on NLTE has been carried out in the temperature range covered by the HgMn stars and, in particular, for the ultraviolet region.

Acknowledgements. We thank grant GO-13346, from the Space Telescope Science Institute, for providing support for the ASTRAL Large Treasury Project.

References

Alecian, G., & Artru, M. C. 1988, in The Impact of Very High S/N Spectroscopy on Stellar Physics, IAU Symp., 132, 235
Alecian, G., & Stift, M. J. 2010, A&A, 516, A53
Alonso-Medina, A., Colón, C., & Rivero, C. 2005, Phys. Scr., 71, 154
Andersen, J., & Jaschek, M. 1984, A&AS, 55, 469
Andersen, J., Jaschek, M., & Cowley, C. R. 1984, A&A, 132, 354
Ansbacher, W., Pinnington, E. H., Kernahan, J. A., & Gosselin, R. N. 1986, Can. J. Phys., 64, 1365
Asplund, M., Grevesse, N., Sauval, A. J., & Scott, P. 2009, ARA&A, 47, 481
Ayres, T. R. 2010, ApJS, 187, 149
Ayres, T. R., et al. 2014, AAS Meeting Abstracts #223, 254.37
Babel, J. 1994, Pulsation; Rotation; and Mass Loss in Early-Type Stars, 162, 333
Bailey, J. D., & Landstreet, J. D. 2013, A&A, 551, A30
Bessell, M. S., & Eggen, O. J. 1972, ApJ, 177, 209
Biemont, E., Morton, D. C., & Quinet, P. 1998, MNRAS, 297, 713
Biémont, É., Blagoev, K., Fivet, V., et al. 2007, MNRAS, 380, 1581
Biémont, É., Blagoev, K., Engström, L., et al. 2011, MNRAS, 414, 3350
Castelli, F. 2005, Mem. Soc. Astron. It. Suppl., 8, 44
Castelli, F., & Hubrig, S. 2007, A&A, 475, 1041
Castelli, F., & Kurucz, R. L. 2010, A&A, 520, A57
Castelli, F., Cornachin, M., & Hack, M. 1981, Liege Int. Astrophys. Colloq., 23, 149
Castelli, F., Cornachin, M., Morossi, C., & Hack, M. 1985, A&AS, 59, 1
Castelli, F., Kurucz, R., & Hubrig, S. 2009, A&A, 508, 401
Castelli, F., Kurucz, R. L., & Cowley, C. R. 2015, A&A, 580, A10
Catanzaro, G., Leone, F., & Dall, T. H. 2004, A&A, 425, 641
Catanzaro, G., Giarrusso, M., Leone, F., et al. 2016, MNRAS, 460, 1999
Cugier, H., & Hardorp, J. 1988, A&A, 197, 163
Curtis, L. J., Matulioniene, R., Ellis, D. G., & Fischer, C. F. 2000, Phys. Rev. A, 62, 052513
Dunlop, J. 1829, MmRAS, 3, 257
Eggen, O. J. 1975, PASP, 87, 37
Enzonga Yoca, S., Biémont, É., Delahaye, F., Quinet, P., & Zeippen, C. J. 2008, Phys. Scr., 78, 025303
Fivet, V., Quinet, P., Biémont, É., & Xu, H. L. 2006, J. Phys. B At. Mol. Phys., 39, 3587
Fuhr, J. R., & Wiese, W. L. 1998, in CRC Handbook of Chemistry and Physics, ed. D. R. Lide (Boca Raton: CRC Press)
Gavrila, M. 1967, Phys. Rev., 163, 147
Ghazaryan, S., & Alecian, G. 2016, MNRAS, 460, 1912
Grevesse, N., Scott, P., Asplund, M., & Sauval, A. J. 2015, A&A, 573, A27
Haris, K., Kramida, A., & Tauheed, A. 2014, Phys. Scr., 89, 115403
Hempel, M., & Holweger, H. 2003, A&A, 408, 1065
Hibbert, A. 1988, Phys. Scr., 38, 37
Holt, R. A., Scholl, T. J., & Rosner, S. D. 1999, MNRAS, 306, 107
Hubrig, S., Castelli, F., & Mathys, G. 1999, A&A, 341, 190
James, D. J., Melo, C., Santos, N. C., & Bouvier, J. 2006, A&A, 446, 971
Jönsson, P., & Andersson, M. 2007, J. Phys. B At. Mol. Phys., 40, 2417
Khalack, V. R., Leblanc, F., Bohlender, D., Wade, G. A., & Behr, B. B. 2007, A&A, 466, 667
Khalack, V. R., Leblanc, F., Behr, B. B., Wade, G. A., & Bohlender, D. 2008, A&A, 477, 641
Kramida, A., Ralchenko, Yu., Reader, J., & NIST ADS Team 2015, NIST Atomic Spectra Database (version 5.3), National Institute of Standards and Technology, Gaithersburg, MD
Kurtz, D. W., & Marang, F. 1995, MNRAS, 276, 191
Kurucz, R. L. 1970, SAO Special Report, 309, 309
Kurucz, R. L. 2005, Mem. Soc. Astron. It. Suppl., 8, 14
Kurucz, R. L. 2016, 21 ASOS Colloq., San Paulo
LeBlanc, F., Khalack, V., Yameogo, B., Thibeault, C., & Gallant, I. 2015, MNRAS, 453, 3766
Leckrone, D. S., Proffitt, C. R., Wahlgren, G. M., Johansson, S. G., & Brage, T. 1999, AJ, 117, 1454
Leone, F. 1998, Contributions of the Astronomical Observatory Skalnate Pleso, 27, 285
Leone, F., & Lanzafame, A. C. 1997, A&A, 320, 893
Leone, F., Catalano, F. A., & Malaroda, S. 1997, A&A, 325, 1125
Ljung, G., Nilsson, H., Asplund, M., & Johansson, S. 2006, A&A, 456, 1181
Michaud, G. 1970, ApJ, 160, 641
Morton, D. C. 2000, ApJS, 130, 403
Nesvacil, N., Shulyak, D., Ryabchikova, T. A., et al. 2013, A&A, 552, A28
Nielsen, K. E., Wahlgren, G. M., Proffitt, C. R., Leckrone, D. S., & Adelman, S. J. 2005, AJ, 130, 2312
Oliver, P., & Hibbert, A. 2010, J. Phys. B At. Mol. Phys., 43, 074013
Peterson, R. C., & Kurucz, R. L. 2015, ApJS, 216, 1

Proffitt, C. R., Brage, T., Leckrone, D. S., et al. 1999, ApJ, 512, 942
Raassen, A. J. J., & Uylings, P. H. M. 1998, A&A, 340, 300
Reader, J., & Acquista, N. 1997, Phys. Scr., 55, 310
Rosberg, M., & Wyart, J.-F. 1997, Phys. Scr., 55, 690
Ryabchikova, T. A., & Smirnov, Y. M. 1994, Astron. Rep., 38, 70
Ryabchikova, T., Wade, G. A., & LeBlanc, F. 2003, in Modelling of Stellar Atmospheres, IAU Symp., 210, 301
Sansonetti, C. J., & Reader, J. 2001, Phys. Scr., 63, 219
Scott, P., Grevesse, N., Asplund, M., et al. 2015a, A&A, 573, A25
Scott, P., Asplund, M., Grevesse, N., Bergemann, M., & Sauval, A. J. 2015b, A&A, 573, A26
Shirai, T., Reader, J., Kramida, A. E., & Sugar, J. 2007, J. Phys. Chem. Ref. Data, 36, 509
Sigut, T. A. A. 2001, ApJ, 546, L115
Smith, K. C. 1993, A&A, 276, 393
Smith, K. C. 1994, A&A, 291, 521
Smith, K. C. 1997, A&A, 319, 928
Smith, K. C., & Dworetsky, M. M. 1993, A&A, 274, 335
Stift, M. J., & Alecian, G. 2012, MNRAS, 425, 2715
Thiam, M., LeBlanc, F., Khalack, V., & Wade, G. A. 2010, MNRAS, 405, 1384
Townley-Smith, K., Nave, G., Pickering, J. C., & Blackwell-Whitehead, R. J. 2016, MNRAS, 461, 73
Uylings, P. H. M., & Raassen, A. J. J. 1997, A&AS, 125, 539
van den Ancker, M. E., de Winter, D., & The, P. S. 1996, A&A, 313, 517
Wiese, W. L., & Martin, G. A. 1980, Wavelengths and transition probabilities for atoms and atomic ions: Part 2. Transition probabilities, NSRDS-NBS, 68
Wyart, J.-F., Joshi, Y. N., Tchang-Brillet, L., & Raassen, A. J. J. 1996, Phys. Scr., 53, 174
Yüce, K., Castelli, F., & Hubrig, S. 2011, A&A, 528, A37

Appendix A: Element-by-element description of the ultraviolet spectrum of HR 6000

A short description of the elements observed in the ultraviolet spectrum of HR 6000 but not considered in the main paper is given in this Appendix.

Boron (B) $Z = 5$: we derived the underabundance [−0.75] from the B II resonance line at 1362.463 Å. It is the main component of a blend with Fe II 1362.451 Å.

Carbon (C) $Z = 6$: see the main paper.

Nitrogen (N) $Z = 7$: see the main paper.

Oxygen (O) $Z = 8$: only the three lines of the O I UV multipet 2 at $\lambda\lambda$ 1302.2, 1304.8, and 1306.0 Å can be observed in the spectrum. The abundance −3.68 dex derived by Castelli et al. (2009) from the optical region fits the lines at 1304.858 Å and 1306.020 Å. The resonance line at 1302.168 Å is blended with a strong interstellar or circumstellar component that is blueshifted by about 0.05 Å, so that only the red part of the profile is closely predicted. Although oxygen is marginally underabundant ([−0.3]), there are only two stars in the Ghazaryan & Alecian (2016) sample with even lower oxygen abundance ([−0.4]).

Magnesium (Mg) $Z = 12$: Castelli et al. (2009) obtained the abundance of −5.66 dex from Mg II at 4481 Å.

The Mg II abundance from the ultraviolet is, on average, 0.25 dex larger, in that it ranges from −5.36 dex to −5.46 dex depending on the lines considered. We used the Mg II lines at 2928.633 Å and 2936.510 Å (mult. 2), those at 2790.777 Å and 2797.998 Å (mult. 3), and the lines at $\lambda\lambda$ 1734.852, 1737.628, and 1753.474 Å. The lines of UV multiplet 1 at 2795.528 Å and 2802.705 Å cannot be used for abundance purposes because they both are contaminated by a very strong interstellar or circumstellar component. Averaging all the abundances from the visual and ultraviolet regions we obtain −5.45 ± 0.09 dex, i.e., an underabundance of [−1.0] that is fully compatible with that of the other HgMn stars of the Ghazaryan & Alecian (2016) sample.

The observed Mg I resonance line at 2852.126 Å is very sharp and much stronger than that computed for −5.36 dex,which is the largest abundance derived from the Mg II lines. It is probably blended with a strong line of interstellar or cicumstellar origin.

Aluminium (Al) $Z = 13$: Castelli et al. (2009) fixed an upper limit for the aluminium abundance of −7.30 dex from the absence of Al I and Al II lines in the UVES spectrum. In the ultraviolet, the resonance line of Al II at 1670.787 Å is blended with a blue interstellar (circumstellar) component, so that it cannot be used. Other lines of Al II are well reproduced by the average abundance of −7.80 ± 0.3 dex. Al III lines at 1854.716 Å and 1862.790 Å are better fitted by the 0.1 dex higher abundance of −7.70 dex. No lines of Al I were clearly detectable. We note that all the lines considered are more or less blended, except perhaps for Al II at 1862.311 Å.

The average abundance from all the Al II and Al III lines listed in Table A.1 is −7.80 ± 0.3 dex, corresponding to an underabundance of [−2.19]. This value is compatible with the underabundances of the HgMn stars of the Ghazaryan & Alecian (2016) sample.

Silicon (Si) $Z = 14$: see the main paper.

Phosphorus (P) $Z = 15$: see the main paper

Sulfur (S) $Z = 16$: a sulfur abundance of −6.26 dex was obtained by Castelli et al. (2009) from the weak unblended S II line at 4162.665 Å. Using the sulfur ultraviolet lines we updated the abundance to −6.36 dex, a value that agrees well with both the ultraviolet S I unblended line at 1425.03 Å and the S II line of UV mult. 1 at 1250.584 Å. The other two lines of S II mult. 1 at 1253.811 Å and 1259.519 Å are too blended with other strong lines, and probably also with some interstellar or circumstellar component, to be used for abundance purposes. All the three strong S II lines of UV mult. 1 lie in a spectral region affected by several uncertainties mostly related with the continuum position and numerous unidentified lines. The sulfur underabundance of [−1.44] puts HR 6000 among the HgMn stars with a very low sulfur abundance according to the Ghazaryan & Alecian (2016) compilation.

Chlorine (Cl) $Z = 17$: the ground-state line of Cl I at 1379.528 Å is absent in the STIS spectrum. For this reason, we adopted as chlorine abundance the upper limit −7.74 dex ([−1.20]) inferred by Castelli et al. (2009) from the absence in the UVES spectrum of the line at 4794.556 Å. Other Cl I lines, if present in the UVES spectrum, are heavy blended with stronger components. Only two stars in the Ghazaryan & Alecian (2016) sample have chlorine abundance. These are χ LupiA and HD 46866 with underabundance [−1.40] and [−0.36], respectively. The underabundance of HR 6000, which is ≤[−1.20], puts the star in between χLupiA and HD 46866.

Calcium (Ca) $Z = 20$: the average calcium abundance obtained from a few ultraviolet unblended lines lying in the region 2110−2210 Å is almost solar (Table A.1). The underabundance of [−0.02] ± 0.09 agrees with the calcium abundance of the HgMn stars of the Ghazaryan & Alecian (2016) sample, which is more or less scattered around the solar value.

Scandium (Sc) $Z = 21$: only weak lines of Sc III were observed in the STIS spectrum. From the unblended line of Sc III at 1603.064 Å an abundance of −10.2 dex was deduced, corresponding to the underabundance of ([−1.11]). There are four stars in the Ghazaryan & Alecian (2016) sample with a scandium underabundance less than that of HR 6000. Therefore, HR 6000 is similar to other HgMn stars as far as the scandium abundance is concerned.

Titanium (Ti) $Z = 22$: Castelli et al. (2009) derived a titanium abundance equal to −6.47 ± 0.13 dex ([+0.64]) from the equivalent widths of numerous Ti II lines observed in the UVES spectrum. This value was confirmed in the ultraviolet by the analysis of several Ti II lines, in particular those at $\lambda\lambda$ 1909.207, 1909.662, and 1910.954 Å. Several Ti III lines of the UV multiplets 1, and 3–7 were examined. There is a large spread in the abundances, which range from −6.0 dex to −7.7 dex (Table A.1). Most lines are blended. In addition, the only source for the log gf values is the Kurucz line list so that we do not have a critical compilation of the Ti III oscillator strengths. The average abundance of Ti II agrees within the error limits with the average Ti III abundance −6.37 ± 0.41 dex. According to the Ghazaryan & Alecian (2016) compilation, the titanium overabundance [+0.64] of HR 6000 is a typical value for HgMn stars.

Vanadium (V) $Z = 21$: the V II lines of multiplets 1, 10, and 12 at 2900 Å are either very weak or not even observed. From three lines at $\lambda\lambda$ 2908.817, 2924.019, and 2924.641 Å, we derived the average abundance of −9.23 ± 0.12 dex. In the Ghazaryan & Alecian (2016) compilation, there are two stars, ΦPhe and HD 71066, with a vanadium underabundance that is lower than the [−1.12] value of HR 6000.

Chromium (Cr) $Z = 24$: the lines of Cr II and Cr III are very numerous in HR 6000. From analyses of the Cr II lines at $\lambda\lambda$ 2055, 2061, 2653, 2666, 2971, and 2989 Å, which are also adopted by Smith & Dworetsky (1993), and of some other unblended lines (Table A.1), we derived an average abundance of −5.9 ± 0.2 dex. This value agrees with the

value of −6.10 ± 0.09 dex obtained from the optical region by Castelli et al. (2009). The Cr III abundance was obtained from a few unblended lines that were extracted by analyzing all the Cr III lines listed in the NIST database for the 1250−3000 Å interval. The average abundance for Cr III is −6.22 ± 0.25 dex. The final chromium abundance −6.10 ± 0.25 dex was obtained averaging the abundances of all the Cr II and Cr III lines examined in both STIS and UVES spectra. According to the Ghazaryan & Alecian (2016) compilation, the chromium overabundance [+0.3] of HR 6000 is a typical value for the HgMn stars.

Manganese (Mn) Z = 25: see the main paper.

Iron (Fe) Z = 26: pratically all the lines of Fe II and Fe III listed in the NIST database are present in the ultraviolet spectrum of HR 6000. A few lines of Fe I, mostly those arising from the ground level, were also identified. The iron abundance −3.65 ± 0.09 dex was carefully determined by Castelli et al. (2009) from several Fe I and Fe II lines observed in the UVES spectrum. We checked that this value closely predicts the ultraviolet Fe II lines used by Smith & Dworetsky (1993) in their analyses of HgMn and related stars (Table A.1). The average abundance from the ultraviolet Fe II lines is −3.68 ± 0.05 dex. This is close to the value of −3.7 ± 0.05 dex obtained by Smith & Dworetsky (1993) for HR 6000.

We extracted a set of unblended lines from the numerous Fe III lines observed in the ultraviolet spectrum (Table A.1). The average abundance −3.78 ± 0.14 dex agrees within the error limits with the Fe II abundance. We finally adopted the value −3.65 ± 0.09 dex deduced by Castelli et al. (2009) from the optical spectrum for the iron abundance of HR 6000. The corresponding iron overabundance, [+0.92], is an upper limit according to the Ghazaryan & Alecian (2016) compilation.

Cobalt (Co) Z = 27: Castelli et al. (2009) estimated an upper limit −8.42 dex (underabundance [−1.3]) for the cobalt abundance from the unobserved Co II line at 3501.708 Å and from the blended Co II line at 4160.657 Å. In the ultraviolet we examined the lines used by Smith & Dworetsky (1993) to derive the cobalt abundance in normal late-B and HgMn stars. They are the lines at $\lambda\lambda$ 2286.159, 2307.86, 2324.321, and 2580.326 Å. We added a few lines listed in Table A.1. While the line at 2307.86 Å is well predicted by −8.42 dex, the other lines, although predicted for this abundance, are not observed. Assuming that the absorption at 2307.86 Å is due to some other unidentified element, we lowered the upper limit of the cobalt abundance to −10.12 dex (underabundance [−3.0]), which suppresses the predicted unobserved lines. Smith & Dworetsky (1993) assigned the upper limit <-9.0 ± 0.5 dex for the cobalt abundance in HR 6000. The cobalt underabundance ≤[−3.0] of HR 6000 is lower than the lower limit given in the Ghazaryan & Alecian (2016) compilation.

Nickel (Ni) Z = 28: Castelli et al. (2009) obtained the abundance −6.24 dex from the equivalent width of the Ni II line at 4067.031 Å. Smith & Dworetsky (1993) derived the nickel abundance in the HgMn stars of their sample from the Ni II lines at $\lambda\lambda$ 2165.550, 2184.602, 2270.212, and 2287.081 Å. For HR 6000 they determined −6.34 dex. In the STIS spectrum the above lines are well fitted by −6.24 dex. The corresponding underabundance is [−0.40]. There are several Ni III lines in the spectrum, but they are all blended except for $\lambda\lambda$ 1774.896, 1829.986, and 1830.060 Å. The average abundance from the three lines quoted above is −6.64 ± 0.14. We adopted as nickel abundance −6.24 dex from Ni II, mostly because Ni II is the dominant ion. According to the Ghazaryan & Alecian (2016) compilation, the nickel underabundance [−0.40] of HR 6000 is a typical value in HgMn stars.

Copper (Cu) Z = 29: Castelli et al. (2009) derived an upper limit for the copper abundance equal to −7.83 dex (solar value) from the Cu II unobserved lines at 4909.734 Å and 4931.698 Å. In the ultraviolet, the abundance −10.53 dex was derived from the Cu II resonance line at 1358.773 Å. The corresponding underabundance is [−2.7]. This value is well below the lower limit of [−0.89] for 112 Her A of the Ghazaryan & Alecian (2016) compilation.

Zinc (Zn) Z = 30: the zinc abundance of −8.84 dex was derived from the very weak Zn II line at 2064.227 Å. In fact, the two strong resonance lines at 2025.502 Å and 2062.004 Å are not useful for this purpose. They both seem to be blueshifted by 0.03 Å and the second line is computed too strong, as compared with the observed line, for −8.84 dex. We argue that the two resonance lines are blended with an interstellar or circumstellar component that affects the profiles in an unpredictable way. We assumed the abundance of −8.84 dex as an upper limit. This abundance corresponds to the underabundance ≤[−1.36], which is consistent with the zinc abundance of the HgMn stars in the Ghazaryan & Alecian (2016) sample.

Gallium (Ga) Z = 31: all the Ga II lines are blended. The abundance −8.85 dex was derived from the Ga II resonance line at 1414.399 Å, which is the main component in a blend. The Ga II resonance line is compatible with that from other subordinate Ga II lines. The resonance lines of Ga III at 1495.045 Å and 1534.462 Å give the lower abundance −8.15 dex, so that there is a discrepancy of −0.65 dex between the Ga II and Ga III abundances. Because Ga II is the dominant state, we assumed for gallium the final abundance of −8.85 dex. The overabundance [+0.17] puts HR 6000 below the lowest overabundance limit equal to [+0.81] ± 0.30 provided by 46 Aql, according to the Ghazaryan & Alecian (2016) compilation.

Germanium (Ge) Z = 32: Ge II lines were not observed in the spectrum. The solar germanium abundance was decreased to to −9.64 dex to fit the spectrum at the position of the ground-configuration line of Ge II at 1649.194 Å. Because the line at 1261.905 is still predicted as a strong line for this abundance, the germanium abundance was further lowered to −10.64 dex.

Arsenic (As) Z = 33: the As II line at 1375.07 Å is predicted for a solar arsenic abundance as minor component in a blend with Ti II which closely fits the observed spectrum. Because other As II lines were neither observed nor predicted, we adopted the solar abundance −9.74 dex for arsenic.

Strontium (Sr) Z = 38: no Sr II lines were observed in the whole spectrum from ultraviolet to the optical regions. We adopted the upper limit −10.07 dex derived from the absence of Sr II at 4077.709 Å. The corresponding underabundance, ≤[−0.9], puts HR 6000 among the most deficient strontium stars of the Ghazaryan & Alecian (2016) sample.

Yttrium (Y) Z = 39: Castelli et al. (2009) obtained the abundance equal to −8.60 dex from the profiles of Y II at $\lambda\lambda$ 3950.349, 4883.682, and 4900.120 Å. However, the strong Y III lines at $\lambda\lambda$ 2367.228, 2414.643, 2817.023, and 2945.995 Å require the higher abundance of −7.6 dex to be fitted. Yttrium overabundance is usual among HgMn stars, with values closer to what we found from Y III than from Y II.

Zirconium (Zr) Z = 40: an upper limit of −10.24 dex was derived from the unobserved Zr III line at 1941.053 Å. The corresponding underabundance ≤[−0.8] contrasts with the usual zirconium overabundance in HgMn stars, as is evident from the Ghazaryan & Alecian (2016) compilation.

Cadmium (Cd) $Z = 48$: the resonance line of Cd II at 2144.393 Å, although blended, is well predicted by the abundance −7.00 dex. The almost unblended Cd II line at 2265.018 Å and two other lines at 2312.766 and 2572.93 Å have intensities that are consistent with this abundance. However, the observed Cd II line at 2748.549 Å is fitted by −7.4 dex. It is also redshifted by 0.007 Å, indicating that the energy levels for this line should be better determined. Cd I at 2288.728 Å is observed, but blended with several features. The most important is Fe II 2288.022 Å. The cadmium overabundance of [+3.33] is a new finding for HR 6000 abundance analyses. In the Ghazaryan & Alecian (2016) sample only χLupi A is quoted for cadmium, which is [+0.56] overabundant in this star.

Indium (In) $Z = 49$: the line of In II at 1586.331 Å is blended with two stronger Fe II lines. The abundance −10.24 dex is not in conflict with the observed blended profile, but In III at 1625.295 Å is predicted as a strong line that is not observed.

Tin (Sn) $Z = 50$: the lines of Sn II are fitted by abundances ranging from −7.0 dex for the line at 2151.514 Å to −8.7 dex for the lines at $\lambda\lambda$1400.440, 1474.997, and 1757.905 Å. However, there are other lines, for example, those at 1312.274 Å and 1899.881 Å which are predicted to be rather strong for −8.7 dex, but are not observed at all. We suspect that incorrect energy levels for Sn II may be responsible. The average abundance is −8.23 ± 0.64 dex. The corresponding overabundance is [+1.77] ± 0.774 dex. The only star with Sn abundance included in the Ghazaryan & Alecian (2016) compilation is χLupi A. The Sn overabundance of this star is <[+1.38], which was derived only from the line at 2151.514 Å (Leckrone et al. 1999).

Xenon (Xe) $Z = 54$: the numerous Xe II lines observed in the optical region yielded the abundance of −5.25 ± 0.17 dex (Yüce et al. 2011). There are no Xe II lines in the ultraviolet spectrum, but two Xe I lines were observed at 1469.612 Å and 1295.588 Å. They give the abundance −5.55 ± 0.25 dex, in agreement with the Xe II value. The xenon overabundance of HR 6000 is similar to that of most HgMn stars of the Ghazaryan & Alecian (2016) sample.

Gold (Au) $Z = 79$: see the main paper.

Mercury (Hg) $Z = 80$: Castelli et al. (2009) derived an abundance of −8.20 dex from a weak structure observed at 3983.9 Å that they interpreted as due to Hg II affected by an isotopic anomaly. However, this abundance cannot be confirmed by the clearly observable Hg II lines at 1649.937 Å and 1942.273 Å, which both yield the abundance of −9.6 dex, i.e., an overabundance of [+1.27]. The lower Hg II abundance is not in conflict with the abundances from a few Hg III lines that are predicted as minor components of blends. An example is Hg III at 1647.471 Å.

In the Ghazaryan & Alecian (2016) compilation only 53 Tau has an overabundance of mercury that is lower than that of HR 6000.

Table A.1. Lines analyzed in the STIS spectrum of HR 6000.

Elem	λ, mult.	log gf	Source[a]	χ_{low}(cm^{-1})	χ_{up}(cm^{-1})	Abund	Notes
B II	1362.463 (1)	−0.001	NIST5	0.000	73 396.510	−10.1	blend Fe II
C I	1277.245 (7)	−1.035	NIST5	0.000	78 293.490	−5.8	
C I	1277.283 (7)	−0.683	NIST5	16.417	783 07.630	−5.8	
C I	1277.513 (7)	−1.169	NIST5	16.417	78 293.490	−5.3	
C I	1277.550 (7)	−0.409	NIST5	43.414	78 318.250	−6.0	
C I	1277.723 (7)	−1.113	NIST5	43.414	78 306.619	−5.5:	blend Fe II
C I	1277.954 (7)	−2.360	NIST5	43.414	78 293.501	−4.9	single
C I	1279.891 (5)	−1.376	NIST5	16.417	78 148.089	−5.10:	blend Cr III, Fe II
C I	1280.135 (5)	−1.583	NIST5	0.000	78 116.748	−5.00	blend Mn II
C I	1280.333 (5)	−1.106	NIST5	43.414	78 148.089	−5.60	single
C I	1280.404 (5)	−1.859	NIST5	16.417	78 116.748	−5.50	blend Mn II
C I	1280.597 (5)	−1.664	NIST5	16.417	78 104.967	−5.10	blend Mn II
C I	1280.847 (5)	−1.573	NIST5	43.414	78 116.748	−5.10	single
C I	1328.833 (4)	−1.236	NIST5	0.000	75 253.983	−5.2	blend Fe II
C I	1329.085 (4)	−1.231	NIST5	16.417	75 256.153	−5.5	
C I	1329.100 (4)	−1.147	NIST5	16.417	75 255.276	−5.5	
C I	1329.123 (4)	−1.355	NIST5	16.417	75 253.983	−5.5	blend Fe III, Fe II
C I	1329.578 (4)	−0.662	NIST5	43.414	75 255.276	−6.0	blend Fe II
C I	1329.600 (4)	−1.136	NIST5	43.414	75 253.983	−6.0	blend Fe II
C I	1560.309 (3)	−1.145	NIST5	0.000	64 089.863	−5.5:	blend Fe II
C I	1560.682 (3)	−0.793	NIST5	16.417	64 090.969	−5.8	blend Fe II
C I	1560.709 (3)	−1.271	NIST5	16.417	64 089.863	−5.8	blend Fe II
C I	1561.340 (3)	−1.271	NIST5	43.414	64 090.969	−6.0	
C I	1561.367 (3)	−2.448	NIST5	43.414	64 089.863	−−	blend, not pred
C I	1561.438 (3)	−0.522	NIST5	43.414	64 086.951	−6.3	
C I	1656.267 (2)	−0.746	NIST5	16.417	60 393.148	−6.7	
C I	1656.928 (2)	−0.844	NIST5	0.000	60 352.639	−5.6	
C I	1657.008 (2)	−0.271	NIST5	43.414	60 393.148	−6.5	
C I	1657.379 (2)	−0.971	NIST5	16.417	60 352.639	−5.5	blend
C I	1657.907 (2)	−0.845	NIST5	16.417	60 333.429	−5.9	blend
C I	1658.121 (2)	−0.748	NIST5	43.414	60 352.639	−6.0	
C II	1323.862 (11)	−1.284	NIST5	74 930.100	150 466.690	−5.5:	no fit
C II	1323.906 (11)	−0.337	NIST5	74 932.620	150 466.690	−5.5:	no fit
C II	1323.951 (11)	−0.144	NIST5	74 930.100	150 461.580	−5.5:	no fit
C II	1323.995 (11)	−1.288	NIST5	74 932.620	150 461.580	−5.5:	no fit
C II	1334.532 (1)	−0.589	NIST5	0.000	74 932.620	−5.0?	wings, blend interstellar comp.
C II	1335.663 (1)	−1.293	NIST5	63.420	74 932.620	−5.0?	wings
C II	1335.708 (1)	−0.335	NIST5	63.420	74 930.100	−5.0?	wings
N I	1310.540 (13)	−0.926	NIST5	28 839.306	105 143.710	−5.6	blend Fe II
N I	1310.943 (13)	−1.205	NIST5	28 838.920	105 119.880	−5.6	blend Fe III
N I	1310.950 (13)	−1.743	NIST5	28 839.306	105 119.880	−5.6	blend Fe III
N I	1411.931 (10)	−1.273	NIST5	28 838.920	99 663.912	−5.9	
N I	1411.939 (10)	−1.916	NIST5	28 839.306	99 663.912	−5.9	
N I	1411.948 (10)	−1.019	NIST5	28 839.306	99 663.427	−5.9	
N I	1492.625 (4)	−0.381	NIST5	19 224.464	86 220.510	−6.8	
N I	1492.820 (4)	−1.360	NIST5	19 233.177	86 220.510	−−	not obs
N I	1494.675 (4)	−0.634	NIST5	19 233.117	86 137.350	−6.8	
N II	1275.038 ( )	−1.206	NIST5	92 237.200	170 666.230	−5.3	
N II	1275.251 ( )	−1.944	NIST5	92 250.300	170 666.230	−5.2	
N II	1276.201 ( )	−1.478	NIST5	92 250.300	170 607.890	−5.2	
N II	1276.225 ( )	−1.948	NIST5	92 251.800	170 607.890	−5.2	
O I	1302.168 (2)	−0.585	NIST5	0.000	76 794.978	−−	blue interstellar comp.
O I	1304.858 (2)	−0.808	NIST5	158.265	76 794.978	−3.68	
O I	1306.029 (2)	−1.285	NIST5	226.977	76 794.978	−3.68	

Notes. For Si II, P II, P III, and S II lines observed in the UVES spectrum by Castelli & Hubrig (2007) are added. The successive columns list: element, wavelength and multiplet number, if available, log gf value, its source, excitation potential of the lower and upper levels, abundance log(N_{elem}/N_{tot}). In the last column some notes are added. [(a)] NIST5= NIST database: http://www.nist.gov/PHYSRefData/ASD/lines-form.html . K16 = Kurucz (2016): http://kurucz.harvard.edu/linelists/gfnew; BMQ = Biemont et al. (1998); Bie = Biémont et al. (2011); Fiv = Fivet et al. (2006); Hi = Hibbert (1988); RW97 = Rosberg & Wyart (1997); YBD = Enzonga Yoca et al. (2008); Proff = Proffitt et al. (1999); SM = Smith & Dworetsky (1993).

Table A.1. continued.

Elem	λ	log gf	Source[a]	χ_{low}(cm^{-1})	χ_{up}(cm^{-1})	Abund	Notes
Mg I	2852.126 (1)	+0.255	NIST5	0.00	35 051.264	−−	strong interstellar comp.
Mg II	1734.852 ( )	−1.111	NIST5	35 669.31	93 311.11	−5.36	blend
Mg II	1737.628 ( )	−0.859	NIST5	35 760.88	93 310.59	−5.46	blend
Mg II	1753.474 ( )	−1.133	NIST5	35 760.88	92 790.51	−5.46:	blend Fe III
Mg II	2790.777 (3)	+0.273	NIST5	35 669.31	71 491.06	−5.36	
Mg II	2795.528 (1)	+0.085	NIST5	0.00	35 760.88	−−	broad violet comp.
Mg II	2797.998 (3)	+0.528	NIST5	35 760.88	71 490.19	−5.36	
Mg II	2802.705 (1)	−0.218	NIST5	0.00	35 669.31	−−	broad violet comp.
Mg II	2928.633 (2)	−0.529	NIST5	35 669.31	69 804.95	−5.46	
Mg II	2936.510 (2)	−0.225	NIST5	35 760.88	69 804.95	−5.46	
Al II	1670.787 (2)	+0.248	NIST5	0.000	59 852.02	−7.80:	strong blue comp
Al II	1719.442 (6)	−0.060	NIST5	37 393.03	95 551.44	−7.30	hfs, blend
Al II	1721.271 (6)	+0.292	NIST5	37 577.79	95 549.42	−7.80	hfs
Al II	1724.982 (6)	+0.565	NIST5	37 453.91	95 550.51	−7.80:	hfs, blend Fe II
Al II	1763.869 (5)	−0.371	NIST5	37 453.91	94 147.46	−7.80	blend
Al II	1763.952 (5)	+0.331	NIST5	37 577.79	94 268.68	−8.30	bl Mn II
Al II	1767.732 (5)	−0.143	NIST5	37 577.79	94 147.46	−7.50	bl Mn II
Al II	1855.926 (4)	−0.886	NIST5	37 393.03	91 274.50	−7.80:	hfs, blend P II
Al II	1858.025 (4)	−0.412	NIST5	37 453.91	91 274.50	−−	too blended Mn II, FeII
Al II	1862.311 (4)	−0.197	NIST5	37 577.79	91 274.50	−8.10	hfs, single
Al III	1854.716 (1)	+0.050	NIST5	0.00	53 916.60	−7.70	blend
Al III	1862.790 (1)	−0.253	NIST5	0.00	53 682.93	−7.70	blend
Si II	1260.422 (4)	+0.387	NIST5	0.000	79 338.50	−−	strong blue component
Si II	1264.738 (4)	+0.639	NIST5	287.240	79 355.02	−8.35 core, −6.65 wings	
Si II	1265.002 (4)	−0.345	NIST5	287.240	79 338.50	−8.35 core, −6.65 wings	
Si II	1304.370 (3)	−0.731	NIST5	0.000	76 665.35	<−8.35	strong blue component
Si II	1305.592 (13.04)	+0.474	K16	55 325.18	131 918.800	−6.40	
Si II	1309.276 (3)	−0.495	NIST5	287.240	76 665.35	−8.35	bl Mn III
Si II	1309.453 (13.04)	+0.318	K16	55 309.35	131 677.100	−6.45	
Si II	1346.884 (7)	−0.389	NIST5	42 932.62	117 178.06	−6.65	bl Mn III
Si II	1348.543 (7)	−0.437	NIST5	42 824.29	116 976.38	−6.65:	blend, blue unident.
Si II	1350.072 (7)	−0.057	NIST5	43 107.91	117 178.06	−8.00?	bl Fe II
Si II	1350.516 (7)	−0.754	NIST5	42 932.62	116 078.38	−6.65	blend
Si II	1350.656 (7)	−0.975	NIST5	42 824.29	116 862.38	−6.65	blend
Si II	1352.635 (7)	−0.474	NIST5	42 932.62	116 862.38	−7.00?	blend Fe III
Si II	1353.721 (7)	−0.451	NIST5	43 107.91	116 978.38	− − −	too blended
Si II	1403.784 (13.03)	−0.961	K16	55 309.35	126 545.400	−6.00	
Si II	1404.482 (13.03)	−0.826	K16	55 325.18	126 525.800	−6.00	
Si II	1409.053 (13.02)	−0.638	NIST5	55 309.35	126 279.000	−6.25	
Si II	1410.214 (13.02)	−0.383	NIST5	55 325.18	126 326.400	−6.25	
Si II	1509.092 (11.01)	−0.410	NIST5	55 325.18	121 590.19	−6.65	single
Si II	1526.707 (2)	−0.575	NIST5	0.000	65 500.47	− − −	strong blue component
Si II	1533.431 (2)	−0.274	NIST5	287.24	65 000.47	−8.35	bl Fe III
Si II	1808.013 (1)	−2.203	NIST5	0.000	55 309.35	−−	blend Fe III+blue comp.?
Si II	1816.928 (1)	−2.103	NIST5	287.240	55 325.18	≤−8.35	not obs !!!!
Si II	1817.451 (1)	−3.194	NIST5	287.240	55 309.35	−−	not obs, not pred for −7.35
Si II	2072.015 (9)	−0.430	NIST5	55 309.35	103 556.16	−7.35:	blend Fe II
Si II	2072.700 (9)	−0.290	NIST5	55 325.18	103 556.030	−7.35:	bl Mn III
Si II	3853.665 (vis 1)	−1.341	NIST5	55 309.35	81 251.32	−7.00	single
Si II	3856.018 (vis 1)	−0.406	NIST5	55 325.18	81 251.32	−7.65	blend unknown?
Si II	3862.595 (vis 1)	−0.757	NIST5	55 309.35	81 191.34	−7.35	single
Si II	4128.054 (vis 3)	+0.359	NIST5	79 338.500	103 556.160	−7.35?	blend
Si II	4130.894 (vis 3)	+0.552	NIST5	79 355.020	103 556.030	−7.40	
Si II	5041.024 (vis 5)	+0.029	NIST5	81 191.34.020	101 023.05	−7.35	weak
Si II	6347.109 (vis 2)	+0.149	NIST5	65 500.47	81 251.32	≤−8.00	not obs?
Si II	6371.371 (vis 2)	−0.082	NIST5	65 500.47	81 191.34	≤−8.00	not obs

Table A.1. continued.

Elem	λ	log gf	Source[a]	χ_{low}(cm^{-1})	χ_{up}(cm^{-1})	Abund	Notes
Si III	1294.545 (4)	−0.173	NIST5	52 853.28	130 100.52	− − −	bl Fe III
Si III	1296.726 (4)	−0.270	NIST5	52 724.69	129 841.97	−7.35	bl uniden.
Si III	1298.892 (4)	−0.396	NIST5	52 853.28	129 841.97	−7.85	blend
Si III	1298.946 (4)	+0.302	NIST5	53 115.01	130 100.52	−7.85:	blend
Si III	1301.149 (4)	−0.272	NIST5	52 853.28	129 708.45	−7.75	blend Fe II
Si III	1303.323 (4)	−0.177	NIST5	53 155.01	129 841.97	−8.35	blend Fe II
Si III	1417.237 (9)	−0.184	NIST5	82 884.41	153 444.23	−6.45	single
Si III	1312.591 (10)	−0.765	NIST5	82 884.41	159 069.61	− − −	blend
Si IV	1393.755 (1)	+0.011	NIST5	0.00	71 784.64	−6.65	blend
Si IV	1402.770 (1)	−0.292	NIST5	0.00	71 287.54	−6.65	single!
P I	1381.476 (2)	+0.081	K16	0.000	72 386.347	−5.45	
P I	1671.671 (2)	−2.805	K16	0.000	59 820.371	−−	not obs
P I	1674.595 (2)	−2.453	K16	0.000	59 715.921	−−	not obs
P I	1679.697 (2)	−2.190	K16	0.000	59 534.549	≤−5.55	not obs
P I	1685.975 (6)	+0.006	K16	11 376.630	70 689.504	−−	blend Fe II
P I	1694.031 (6)	−0.149	K16	11 361.020	70 391.801	−−	blend, wrong Fe II
P I	1774.949 (1)	−0.211	NIST5	0.000	56 339.656	−5.60	bad fit, blue comp?
P I	1782.829 (1)	−0.389	NIST5	0.000	56 090.626	−5.60	blend
P I	1787.648 (1)	−0.690	NIST5	0.000	55 939.421	−5.50	
P I	1858.871 (5)	−1.142	NIST5	11 361.020	65 157.126	−5.60	
P I	1858.901 (5)	−0.279	NIST5	11 361.020	65 156.242	−5.60	
P I	1859.410 (5)	−0.086	NIST5	11 376.630	65 157.126	−5.60	blend Fe II
P I	1859.441 (5)	−1.209	K16	11 376.630	65 156.242	−−	too blended
P I	2135.469 (4)	−1.076	K16	11 361.020	58 174.366	≤−5.50	not obs
P I	2136.182 (4)	−0.114	NIST5	11 376.630	58 174.366	−5.50	single
P I	2149.142 (4)	−0.211	K16	11 361.020	57 876.574	−5.35	single
P II	1301.874 (2)	−1.42	NIST5	0.000	76 812.330	−4.45:	blend
P II	1304.492 (2)	−1.42	NIST5	164.900	76 823.110	−4.45:	blend
P II	1304.675 (2)	−1.55	NIST5	164.900	76 812.330	−4.45:	blend
P II	1305.497 (2)	−1.31	NIST5	164.900	76 764.060	−4.45:	blend
P II	1309.874 (2)	−2.215	K16	469.120	76 812.330	−4.45:	blend
P II	1310.703 (2)	−0.85	NIST5	469.120	76 764.060	−4.45:	blend
P II	1452.900 ( )	−1.331	HI	8882.310	77 710.19	−4.55	blend Fe II
P II	1485.496 ( )	−0.825	K16	21575.63	88 893.22	−4.55	from red wing
P II	1532.533 (1)	−2.122	K16	0.000	65 251.450	−4.45	blend
P II	1535.923 (1)	−1.765	K16	164.900	65 272.350	−4.45	blend
P II	1536.416 (1)	−2.274	K16	164.900	65 251.450	−4.45	blend
P II	1542.304 (1)	−1.501	K16	469.120	65 307.170	−4.45	blend
P II	1543.051 ( )	−1.645	K16	65 251.45	130 058.110	−4.80	
P II	1543.133 (1)	−2.295	K16	469.120	65 272.350	−4.45	blend
P II	1543.631 (1)	−3.496	K16	469.120	65 251.450	−4.45	blend
P II	1685.850 ( )	−0.301	K16	881 92.130	147 509.39	−4.70	
P II	1858.209 ( )	+0.048	K16	88 192.130	142 007.39	−4.70	blend
P II	2280.991 (6)	+0.182	K16	87 804.100	121 631.16	−−	too blended
P II	2285.105 (7)	+0.466	K16	88 192.130	131 940.29	−4.60	single
P II	2497.372 (5)	−1.089	K16	65 272.35	105 302.37	−4.45	single
P II	4044.576 (30)	+0.669	K16	107 360.25	132 077.74	−4.60	single, 4044.595?
P II	4062.149 (17)	−0.637	K16	103 339.14	127 949.70	−4.75	single
P II	4072.289 (16)	−1.074	K16	103 339.14	127 888.42	−4.60	single
P II	4127.559 (16)	+0.006	K16	103 667.86	127 888.42	−4.65	single
P II	4160.623 (31)	−0.760	K16	103 339.14	127 367.23	−4.65	single
P II	4244.622 (30)	−0.412	K16	130 912.84	107 360.25	−4.65	single
P II	4288.606 (33)	−1.118	K16	101 635.69	124 946.73	−4.65:	blend Fe II
P II	4420.712 ( )	−0.395	K16	88 893.22	111 597.66	−4.50	single

Table A.1. continued.

Species	λ(Å)	log gf	Source[a]	$\chi_{\rm low}$	$\chi_{\rm up}$	log(N_Z)/$N_{\rm tot}$)	Notes
P II	4452.472 (31)	−0.083	K16	105 302.37	127 755.500	−4.60	single
P II	4463.027 (25)	+0.164	K16	105 549.67	127 949.700	−4.60	single
P II	4466.140 (24)	−0.483	K16	105 549.67	127 934.090	−4.65	single
P II	4468.000 (25)	+0.010	K16	105 224.060	127 599.160	−4.65	blend
P II	4475.270 (24)	+0.535	K16	105 549.670	127 888.420	−4.65	single
P II	4483.693 (25)	−0.644	K16	105 302.370	127 599.160	−4.50	single
P II	4499.230 ( )	+0.614	K16	107 922.930	130 142.720	−4.60	single
P II	4927.197 (13)	−0.799	K16	103 165.610	123 455.460	−4.50	single
P II	4943.497 (13)	+0.082	K16	103 667.860	123 890.810	−4.40	single
P II	4954.367 (13)	−0.501	K16	103 165.610	123 344.190	−4.40	single
P II	4969.701 (13)	−0.174	K16	103 339.140	123 455.460	−4.40	single
P II	5152.221 (7)	−1.395	K16	86 597.550	106 001.250	−4.60	single
P II	5191.393 (7)	−0.675	K16	86 743.960	106 001.250	−4.40	single
P II	5296.077 (7)	−0.053	K16	87 124.600	106 001.250	−4.25	single
P II	5316.055 (6)	−0.291	K16	86 743.960	105 549.670	−4.30	bl
P II	5344.729 (6)	−0.280	K16	86 597.550	105 302.370	−4.25	
P II	5386.895 (6)	−0.257	K16	86 743.960	105 302.370	−4.30	
P II	5409.722 (6)	−0.312	K16	86 743.960	105 224.060	−4.30	
P II	5425.880 (6)	+0.288	K16	87 124.600	105 549.670	−4.30	core not fitted
P II	5450.709 (23)	+0.083	K16	105 549.670	123 890.810	−4.45	
P II	5499.697 (6)	−0.441	K16	87 124.600	105 302.370	−4.35	
P II	5507.174 (23)	−0.559	K16	105 302.370	123 455.460	−4.45	bl
P II	5541.139 (23)	−0.515	K16	105 302.370	123 344.190	−4.45	
P II	5583.235 (23)	−0.508	K16	105 549.670	123 455.460	−4.50	
P II	6024.178 (5)	+0.198	K16	86 743.960	103 339.140	−4.20	core not fitted
P II	6034.039 (5)	−0.151	K16	86 597.550	103 165.610	−4.20	core not fitted
P II	6043.084 (5)	+0.442	K16	87 124.600	103 667.860	−4.25	core not fitted
P II	6087.837 (5)	−0.381	K16	86 743.960	103 165.610	−4.30	
P II	6165.598 (5)	−0.412	K16	87 124.600	103 339.140	−4.30	
P III	1334.813 (1)	−1.168	K16	0.000	74 916.85	−−	blend
P III	1344.326 (1)	−0.931	K16	559.140	74 945.86	−−	blend
P III	1344.850 (1)	−1.958	K16	559.140	74 916.85	−4.80	from the red wing, blend
P III	1379.912 (7)	−2.170	K16	74 916.85	147 385.26	≤−5.54	not obs
P III	1380.464 (7)	−1.012	K16	74 945.86	147 385.26	−5.00	blend
P III	1381.095 (7)	−1.225	K16	74 916.86	147 323.19	≤−5.54	blend
P III	1381.648 (7)	−2.046	K16	74 945.86	147 323.19	−−	too blended
P III	4059.340 (1)	−0.236	K16	116 885.87	141 513.63	−4.70	
P III	4080.100 (1)	−0.494	K16	116 874.56	141 376.91	−4.70	
P III	4222.232 (3)	+0.218	K16	117 835.95	141 513.63	−4.55	
P III	4246.750 (3)	−0.086	K16	117 835.95	141 376.91	−4.80	single
S I	1425.030 (5)	−0.094	NIST5	0.000	70 173.968	−6.26	single
S I	1433.278 (5)	−0.365	NIST5	396.055	70 166.195	−6.90	
S I	1436.967 (5)	−0.716	NIST5	573.64	70 164.658	>−−	λ?, bl unknown?, bl Fe II
S I	1448.229 ( )	−0.326	NIST5	9238.069	78 288.44	−−	blend Fe II
S I	1472.971 (4)	−1.071	NIST5	0.000	67 890.016	−−	not obs
S I	1473.995 (3)	−0.349	NIST5	0.000	67 842.967	−−	bl Fe II
S I	1474.378 (3)	−1.10	NIST5	0.000	67 825.188	−−	bl Fe II
S I	1474.571 (3)	−2.278	NIST5	0.000	67 816.351	−−	not obs
S I	1481.663 (4)	−1.536	K16	396.055	67 887.805	−−	not obs
S I	1483.038 (3)	−0.624	NIST5	396.055	67 825.188	−6.36	weak, bl Fe III
S I	1483.233 (3)	−1.101	NIST5	396.055	67 816.315	−−	bl unknown?
S I	1485.622 (4)	−2.638	NIST5	573.64	67 885.535	−−	not obs
S I	1487.150 (3)	−0.979	NIST5	573.640	67 813.351	−6.90	bl Au III
S I	1666.687 (11)	−0.021	NIST5	9238.609	69 237.886	−−	bl Fe II
S I	1807.318 (2)	−0.319	NIST5	0.000	55 330.811	>−6.26?	bl Mn II
S I	1820.343 (2)	−0.593	NIST5	396.055	55 330.811	−−	bl Mn II
S I	1826.245 (2)	−1.073	NIST5	373.640	55 330.811	−−	bl Fe III

Table A.1. continued.

Elem	λ	log gf	Source[a]	χ_{low}(cm^{-1})	χ_{up}(cm^{-1})		Abund	Notes
S II	1250.584 (1)	−1.618	NIST5	0.000	79 962.61	−6.36	blend	
S II	1253.811 (1)	−1.315	NIST5	0.000	79 756.83	>−6.26	blend Mn II	
S II	1259.519 (1)	−1.138	NIST5	0.000	79 395.39	−6.26	bl Fe II	
S II	1363.031 ( )	−2.638	NIST5	24 524.83	97 890.74	<−5.70	blend Fe II	
S II	1363.376 ( )	−2.357	NIST5	24 571.54	97 918.86	−5.70	blend Fe II	
S II	4162.665 (1)	+0.780	NIST5	128 599.16	152 615.46	−6.36	single	
Cl I	1335.572 (2)	−0.755	K16	0.00	74 865.667	−−	bl C II	
Cl I	1347.240 (2)	−0.341	NIST5	0.00	74 225.846	−6.85	blend	
Cl I	1351.656 (2)	−0.486	K16	882.352	74 865.667	−7.75	blend	
Cl I	1363.447 (2)	−0.835	K16	882.352	74 225.846	−7.75?	blend	
Cl I	1379.528 (1)	−1.722	K16	0.00	72 488.568	−−	not obs	
Cl I	1389.957 (1)	−3.010	NIST5	882.352	72 827.038	−−	not obs	
Cl I	1396.527 (1)	−2.629	NIST5	882.352	72 488.568	−−	not obs	
Ca II	2112.757 (9)	−0.409	K16	25 414.40	72 730.93	−5.80	single	
Ca II	2113.146 (9)	−1.364	K16	25 414.40	72 722.23	−5.80	single	
Ca II	2131.505 (3)	−2.310	NIST5	13 710.88	60 611.28	−5.68	blend	
Ca II	2197.787 (8)	−1.303	K16	25 191.51	70 677.62	−5.60	single	
Ca II	2208.611 (8)	−1.004	K16	25 414.40	70 677.62	−5.60	single	
Sc III	1598.001 (1)	−1.239	K16	0.00	62 578.18	≤−10.2		
Sc III	1603.064 (1)	−0.285	K16	197.64	62 578.18	−10.2	single	
Sc III	1610.194 (1)	−0.543	K16	197.64	62 104.30	−9.6		
Sc III	2699.066 ( )	+0.080	K16	25 539.32	62 578.18	−10.2	blend	
Ti II	1909.207 ( )	−0.321	K16	94.114	52 471.895	−6.46	blend	
Ti II	1909.662 ( )	−0.132	K16	94.114	52 459.395	−6.46	blend	
Ti II	1910.954 ( )	−0.407	NIST5	0.000	52 329.889	−6.46	blend	
Ti III	1295.884 (1)	−0.439	K16	0.000	77 167.43	−6.46	blend	
Ti III	1298.633 (1)	−0.906	K16	420.400	77 424.45	−6.46	blend	
Ti III	1298.697 (1)	−0.271	K16	0.000	77 000.23	−6.46	blend	
Ti III	1298.996 (1)	−0.210	NIST5	184.900	77 167.43	−6.46	blend	
Ti III	1327.609 (4)	−0.538	K16	8473.500	83 796.86	−6.46	blend Fe II	
Ti III	1455.195 (5)	+0.233	K16	14 397.600	83 116.93	−6.1	blend	
Ti III	1498.695 (3)	−0.238	K16	8473.500	75 198.21	−6.0	blend Fe II	
Ti III	2374.99 (10)	−0.003	K16	41 704.270	83 796.86	−6.46	blend Fe II	
Ti III	2527.845 (7)	+0.138	K16	38 198.95	77 746.94	−6.0	blend Mn II	
Ti III	2540.048 (7)	−0.065	K16	38 064.35	77 421.86	−6.26	blend Fe II	
Ti III	2565.408 (6)	−0.146	K16	38 198.950	77 167.43	−6.0	single	
Ti III	2567.556 (6)	−0.118	K16	38 064.350	77 000.23	−6.1	λ = 2567.54?, single	
Ti III	2576.463 (6)	−0.521	K16	38 198.950	77 000.23	−6.3	blend Fe II	
Ti III	2984.744 (8)	+0.171	K16	41 704.270	75 198.21	−7.7	blend Fe II	
V II	2908.817 (12)	+0.310	K16	3162.966	37 531.132	−9.14	blend	
V II	2924.019 (10)	+0.420	K16	3162.966	37 352.464	−9.40	blend	
V II	2924.641 (10)	+0.810	K16	2968.389	37 150.615	−9.14	blend	
Cr II	2055.599 (1)	−0.186	K16	0.000	48 632.059	−6.1	single	
Cr II	2061.577 (1)	−0.312	K16	0.000	48 491.057	−6.1	bl Fe III	
Cr II	2653.581 (8)	−0.617	K16	12 032.545	49 706.261	−6.1	bl Fe II, Mn II	
Cr II	2666.014 (8)	−0.106	K16	12 147.771	49 645.806	−5.9	blend	
Cr II	2858.910 (5)	−0.224	K16	12 496.457	47 464.557	−5.9	single	
Cr II	2860.931 (5)	−0.449	K16	11 961.746	46 905.137	−5.7	single	
Cr II	2862.569 (5)	−0.070	K16	12 303.820	47 227.291	−5.8	single	
Cr II	2971.901 (80)	+0.523	K16	30 391.831	54 030.505	−5.7	single	
Cr II	2989.190 (80)	+0.237	K16	30 156.734	63 600.861	−5.8	single	

Table A.1. continued.

Elem	λ	log gf	Source[a]	χ_{low}(cm^{-1})	χ_{up}(cm^{-1})	Abund	Notes
Cr III	1261.865 (20)	−0.649	K16	208 51.87	100 099.66	−5.90	
Cr III	1263.611 (20)	−0.765	K16	20 702.45	99 840.73	−6.60	
Cr III	1268.021 (5)	−1.309	K16	17 850.13	96 713.15	−6.6	single
Cr III	1696.642 (71)	+0.835	K16	94 375.18	153 315.13	≤−6.6	not obs
Cr III	1827.336 (46)	−0.846	K16	56 650.51	111 374.97	−6.3	single
Cr III	2203.228 (47)	+0.236	K16	63 420.87	108 794.65	−6.2	single
Cr III	2226.679 (39)	+0.631	K16	50 409.28	95 305.25	−5.9	single
Cr III	2277.483 (67)	+0.384	K16	71 676.22	115 570.79	−6.5	single
Cr III	2319.074 (44)	+0.414	K16	56 992.24	100 099.66	−5.9	single
Cr III	2483.073 (43)	+0.192	K16	57 422.53	97 683.060	−6.0	single
Cr III	2531.023 (42)	−0.484	K16	56 650.51	96 148.35	−6.3	single
Cr III	2537.756 (42)	−0.509	K16	56 992.24	96 385.29	−6.1	single
Cr III	2544.373 (42)	−0.710	K16	57 422.53	96 713.15	−6.1	single
Cr III	2564.774 (39)	−0.401	K16	74 787.89	113 766.00	−6.2	single
Cr III	2640.737 (65)	−0.443	K16	71 676.22	109 533.15	−6.1	single
Mn II	1382.301 (14)	−1.568	K16	14 593.835	86 936.98	−5.40	hfs, single
Mn II	1383.049 (14)	−1.842	K16	14 593.835	86 897.932	−5.55	hfs, single
Mn II	1385.890 (14)	−1.753	K16	14 781.205	86 936.98	−5.30	hfs, blend
Mn II	1853.266 (12)	−0.230	K16	14 325.866	68 284.664	−5.80	hfs, single
Mn II	1868.585 ( )	−1.492	K16	14 901.203	68 417.697	−5.30	hfs, bl Fe III
Mn II	1911.409 (10)	−0.407	NIST5	14 325.866	66 643.296	−5.30	hfs, blend
Mn II	1923.339 (11)	−1.053	NIST5	14 901.203	66 894.13	−5.30	hfs, single
Mn II	1925.511 (11)	−1.069	NIST5	14 959.876	66 894.130	−5.30	hfs, bl Fe III
Mn II	1926.577 (10)	−0.700	NIST5	14 781.205	66 686.739	−5.30	hfs, single
Mn II	1926.945 (10)	−1.324	NIST5	14 781.205	66 676.833	−5.40	hfs, bl Fe III
Mn II	2535.977 ( )	−1.045	NIST5	27 588.534	67 002.217	−5.30	hfs, single
Mn II	2576.104 (1)	+0.399	NIST5	0.000	38 806.691	−5.30	hfs, bl Mn II, core
Mn II	2593.721 (1)	+0.290	NIST5	0.000	38 543.122	−5.30	hfs, bl Fe II, core
Mn II	2605.680 (1)	+0.137	NIST5	0.000	38 366.232	−5.30	hfs, bl Mn II, core
Mn II	2701.698 (18)	+0.608	K16	27 547.260	64 550.040	−5.30	hfs, bl Fe II, Cr II, core
Mn II	2705.730 (18)	+0.479	K16	27 571.250	64 518.890	−5.30	hfs, single, core
Mn II	2708.449 (18)	+0.219	K16	27 583.590	64 494.140	−5.30	hfs, bl Fe II, core
Mn II	2710.334 (18)	+0.213	K16	27 588.534	64 473.421	−5.30	hfs, single, core
Mn II	2711.562 (18)	−0.525	K16	27 588.534	64 456.720	−5.30	hfs, single, core
Mn II	2711.623 (18)	+0.100	K16	27 589.360	64 456.720	−5.30	hfs, single, core
Mn II	2933.054 (5)	−0.102	NIST5	9472.993	43 557.175	−5.30	hfs, single, core
Mn II	2933.785 ( )	−1.458	NIST5	32 818.440	66 894.130	−5.30	hfs, single
Mn II	2935.362 ( )	−2.002	NIST5	32 836.740	66 894.130	−5.30	hfs, single
Mn II	2939.308 (5)	+0.108	NIST5	9472.993	43 484.664	−5.30	hfs, single, core
Mn II	2949.204 (5)	+0.253	NIST5	9472.993	43 370.527	−5.30	hfs, bl Fe II, core
Mn III	1283.580 (9)	−0.251	K16	43 573.160	121 480.240	−5.9	λ 1283.564?
Mn III	1287.584 (9)	−0.429	K16	43 602.500	121 267.320	−5.9	blend
Mn III	1972.869 (12)	−0.603	K16	62 747.500	113 676.530	−5.90	single
Mn III	1975.451 (12)	−0.614	K16	62 456.990	113 078.340	−6.00	blend
Mn III	1986.853 (12)	−0.807	K16	62 747.500	113 078.340	−5.55	blend Fe III
Mn III	2013.519 (17)	−0.552	K16	71 831.980	121 480.240	−6.2	blend Mn III
Mn III	2016.333 (17)	−0.522	K16	71 395.270	120 974.250	−6.4	single
Mn III	2018.455 (17)	−0.304	K16	71 564.210	121 091.080	−6.2	single
Mn III	2026.938 (11)	−0.465	K16	62 456.990	111 776.600	−5.55	blend
Mn III	2027.106 (11)	−0.736	K16	62 568.080	111 883.600	−5.55	single, λ = 2027.125?
Mn III	2027.872 (17)	+0.345	K16	71 823.330	121 480.240	−6.10	blend
Mn III	2029.428 (17)	−0.317	K16	71 831.980	121 091.080	−6.30	single
Mn III	2031.515 (11)	−0.260	K16	62 568.080	111 776.600	−5.55	blend
Mn III	2036.670 (17)	−0.376	K16	72 183.330	121 267.320	−6.30	single
Mn III	2049.682 ( )	+0.331	K16	63 285.370	112 057.800	−4.90	single
Mn III	2077.369 (10)	+0.410	K16	62 988.920	111 111.390	−5.30	bl Fe II

Table A.1. continued.

Elem	λ	log gf	Source[a]	χ_{low}(cm^{-1})	χ_{up}(cm^{-1})	Abund	Notes
Mn III	2094.773 (10)	−0.026	K16	62 988.920	110 711.620	−5.30	single
Mn III	2106.012 ( )	−0.830	K16	62 568.080	110 036.140	−5.80	single
Mn III	2215.233 (16)	+0.153	K16	71 564.210	116 692.150	−6.00	single
Mn III	2220.558 ( )	+0.330	K16	71 831.980	116 851.690	−5.60	blend
Mn III	2220.743 ( )	−0.494	K16	71 564.210	116 580.170	−5.90	single
Mn III	2354.663 (15)	−0.834	K16	71 564.210	116 692.150	−5.60	single
Mn III	2374.314 (15)	−0.171	K16	72 183.330	114 287.910	−5.55	single, λ = 2374.33?
Mn III	2408.086 (14)	−0.551	K16	71 564.210	113 078.340	−5.90	single
Mn III	2423.720 (14)	−0.323	K16	71 831.980	113 078.340	−5.40	single, λ = 2423.735?
Fe I	2966.898 (1)	−0.404	NIST5	0.00	33 695.397	−3.74	
Fe I	2973.132 (1)	−0.901	NIST5	704.007	34 328.752	−3.74	
Fe I	2973.235 (1)	−0.660	NIST5	415.933	34 039.516	−3.74	
Fe II	2598.369 (1)	−0.062	NIST5	384.787	38 858.97	−3.74	SM
Fe II	2607.087 (1)	−0.152	NIST5	667.683	39 013.216	−3.74	SM
Fe II	2611.873 (1)	−0.009	NIST5	384.787	38 660.054	−3.74	SM
Fe II	2613.824 (1)	−0.362	NIST5	862.612	39 109.316	−3.74	SM
Fe II	2617.617 (1)	−0.522	NIST5	867.683	38 858.97	−3.64	SM
Fe II	2621.669 (1)	−0.938	NIST5	977.050	39 109.316	−3.64	SM
Fe II	2628.293 (1)	−0.441	NIST5	977.050	39 013.216	−3.64	SM
Fe II	2730.734 (62)	−0.900	NIST5	8680.471	45 289.825	−3.64	SM
Fe II	2743.197 (62)	−0.051	NIST5	8846.784	45 289.825	−3.65	blend
Fe II	2755.736 (62)	+0.389	NIST5	7955.319	44 232.540	−3.64	blend
Fe III	1468.982 ( )	−1.471	K16	50 275.840	118 350.20	−3.00	single?
Fe III	1854.395 ( )	−0.564	K16	83 647.000	137 572.94	−3.90	single
Fe III	1882.369 ( )	+0.160	K16	89 783.550	142 908.100	−3.90	single
Fe III	1883.208 ( )	−0.913	K16	87 901.860	141 002.750	−3.64	single
Fe III	1904.265 ( )	+0.157	K16	109 570.800	162 084.49	−3.90	single
Fe III	1924.125 ( )	+0.098	K16	97 041.300	149 012.98	−3.90	single
Fe III	1945.344 ( )	+0.359	K16	69 836.890	121 241.69	−3.80	single
Fe III	1946.766 ( )	+0.345	K16	114 351.930	165 719.17	−3.80	single
Fe III	1951.331 ( )	−0.702	K16	70 694.170	121 941.23	−3.90	single
Fe III	1958.744 ( )	−0.030	K16	89 697.470	140 750.59	−3.64	single
Fe III	1961.014 ( )	+0.112	K16	90 472.370	141 466.39	−3.80	single
Fe III	1961.727 ( )	−0.471	K16	90 423.540	141 399.04	−3.90	single
Fe III	1994.087 ( )	+0.351	K16	63 487.080	113 635.34	−3.90	single
Fe III	1994.377 ( )	−1.669	K16	63 494.380	113 635.34	−3.40	single
Fe III	2053.527 ( )	−0.768	K16	76 956.760	125 637.87	−3.70	single
Fe III	2057.936 ( )	+0.184	K16	97 041.300	145 681.13	−3.70	single
Fe III	2087.145 ( )	+0.189	K16	76 956.760	124 853.86	−3.64	single
Fe III	2103.818 ( )	+0.175	K16	70 728.930	118 246.49	−3.8	single
Fe III	2107.337 ( )	+0.149	K16	70 725.220	118 163.44	−3.9	single
Co II	2011.516 ( )	−0.480	NIST5	0.000	49 697.683	≤−10.12	not obs
Co II	2022.354 ( )	−0.490	NIST5	950.324	50 381.724	≤−10.12	not obs
Co II	2025.759 ( )	−0.950	NIST5	0.000	49 308.304	≤−10.12	not obs
Co II	2286.159 (9)	+0.530	NIST5	3350.494	47 078.491	≤−10.12	not obs
Co II	2307.860 (9)	+0.360	NIST5	4028.988	47 345.842	−8.42	blend
Co II	2324.321 (8)	−0.350	NIST5	4028.988	47 039.102	≤−10.12	blend
Co II	2580.326 (14)	+0.360	NIST5	9812.859	48 556.049	−10.12	blend
Ni II	2165.550 (12)	+0.253	K16	8393.900	54 557.05	−6.24	
Ni II	2184.602 ( )	−0.031	K16	10 663.890	56 424.49	−6.24	
Ni II	2270.212 ( )	+0.120	K16	9330.04	53 365.17	−6.24	blend Fe II
Ni II	2287.081 ( )	+0.020	K16	14 995.57	58 705.95	−6.24	blend
Ni II	2312.917 ( )	+0.521	K16	32 499.53	75 721.68	−6.24	single

Table A.1. continued.

Elem	λ	log gf	Source[a]	χ_{low}(cm^{-1})	χ_{up}(cm^{-1})	Abund	Notes
Ni III	1794.896 ( )	−0.103	K16	54 657.83	110 371.35	−6.44	single
Ni III	1829.986 ( )	+0.207	K16	61 338.58	116 191.93	−6.74	single
Ni III	1830.060 ( )	+0.054	K16	63 471.93	118 114.95	−6.74	single
Cu II	1358.773 (3)	−0.174	K16	0.00	73 595.813	−10.53	single
Zn II	2064.227 (4)	+0.070	NIST5	48 481.077	96 909.893	−8.84	single
Ga II	1414.399 (2)	+0.248	NIST5	0.00	70 701.427	−8.85	blend
Ga III	1495.045 ( )	+0.033	NIST5	0.00	66 887.630	−8.16	blend
Ga III	1534.462 ( )	−0.281	NIST5	0.00	65 169.400	−8.16	blend
Ge II	1261.905 (4)	+0.500	NIST5	1767.357	81 012.598	≤−10.64	not obs
As II	1375.074 (4)	+0.000	BMQ	10 095.082	82 819.214	−9.74	blend
Y III	2414.643 (1)	−0.290	Bie	0.00	41 401.46	−7.6	single
Y III	2945.995 (3)	−0.150	Bie	7467.10	41 401.46	−7.6	single
Zr III	1941.053 (18)	−0.036	NIST5	8839.97	60 358.40	≤−10.24	not obs
Cd I	2288.728 ( )	+0.100	NIST5	0.00	43 692.389	−−	blend
Cd II	2144.393 ( )	−0.110	NIST5	0.00	46 618.532	−7.00	blend
Cd II	2265.018 ( )	−0.340	NIST5	0.00	44 136.080	−7.00	single
Cd II	2572.930 ( )	−0.470	NIST5	44 136.08	82 990.660	−7.00	blend
Cd II	2748.549 ( )	−0.200	NIST5	46 618.55	82 990.660	−7.40	single, λ = 2748.556 Å
In II	1586.331 ( )	+0.160	NIST5	0.000	63 038.546	−10.24	blend
Sn II	1290.875 ( )	+0.470	NIST5	4251.494	81 718.300	−7.80	single
Sn II	1316.581 ( )	+0.050	NIST5	0.000	75 954.300	−8.50	blend
Sn II	1400.440 ( )	+0.380	NIST5	0.000	71 406.142	−8.70	blend
Sn II	1474.997 ( )	+0.580	NIST5	4251.494	72 048.26	−8.70	blend
Sn II	1757.905 ( )	−0.550	NIST5	0.000	56 885.895	−8.70	single
Sn II	2151.514 ( )	−2.530	NIST5	0.000	46 464.29	−7.00	single
Xe I	1295.588 ( )	−0.730	NIST5	0.000	77 185.041	−6.00	single
Xe I	1469.612 ( )	−0.564	NIST5	0.000	68 045.156	−5.10	blend
Au II	1469.142 ( )	−1.470	Fiv	17 640.616	85 707.570	−8.20	blend Fe III
Au II	1673.587 ( )	−0.130	Fiv	15 039.572	74 791.477	−8.00	blend Fe III
Au II	1740.475 ( )	+0.230	Fiv	15 039.572	72 495.129	−7.70	single
Au II	1749.756 ( )	−0.330	Fiv	17 640.616	74 791.477	−8.00	blend
Au II	1756.098 ( )	−0.290	Fiv	29 621.249	86 565.667	−8.20	blend Fe II
Au II	1783.199 ( )	+0.100	Fiv	29 621.249	85 700.201	−8.20	
Au II	1793.297 ( )	−0.050	RW97	17 640.616	73 403.839	−8.20	strong, blend Fe II
Au II	1800.579 ( )	−0.060	Fiv	17 640.616	73 178.291	−6.30	blended unknown?
Au II	1823.220 ( )	−0.670	Fiv	27 765.758	82 613.781	−−	too blended Mn II
Au II	1921.651 ( )	−0.620	Fiv	29 621.249	81 659.828	−8.20	blend
Au II	2000.792 ( )	−0.350	Fiv	15 039.572	65 003.594	−7.50	single
Au II	2082.074 (1)	−0.090	Fiv	15 039.572	63 053.318	−7.50	single
Au III	1278.521 ( )	−0.610	YBD	40 345.900	118 561.300	<−10.00	very weak
Au III	1290.028 ( )	−0.940	YBD	44 425.900	121 943.600	−8.50	
Au III	1291.983 ( )	−0.610	YBD	44 425.900	121 826.300	≤−10.0	not obs
Au III	1314.833 ( )	−0.740	YBD	29 754.00	105 809.100	≤−10.0	blend P II wrong
Au III	1336.707 ( )	+0.180	YBD	29 754.00	104 564.600	−−	blend Fe II
Au III	1348.879 ( )	−0.600	YBD	44 425.900	118 561.300	−8.70	weak single
Au III	1350.307 ( )	−0.560	YBD	38 822.400	112 879.700	≤−10	
Au III	1353.206 ( )	−0.690	YBD	44 425.900	118 324.500	−8.50	λ = 1353.990?
Au III	1365.382 ( )	+0.500	YBD	29 754.000	102 993.000	−9.00	λ = 1365.375?
Au III	1385.768 ( )	+0.190	YBD	38 822.400	110 984.600	−9.00	λ = 1385.78?
Au III	1487.130 ( )	−0.140	YBD	35 076.900	102 320.500	−9.30	
Au III	1746.057 ( )	−0.220	YBD	38 822.400	96 097.700	−8.60	weak single
Hg II	1649.937 (1)	+0.290	NIST5	0.00	60 608.362	−9.60	
Hg II	1942.273 (1)	−0.418	Proff	0.00	51 486.070	−9.60	hfs